Cell

Article

Glia-like taste cells mediate an intercellular mode of peripheral sweet adaptation

Graphical abstract

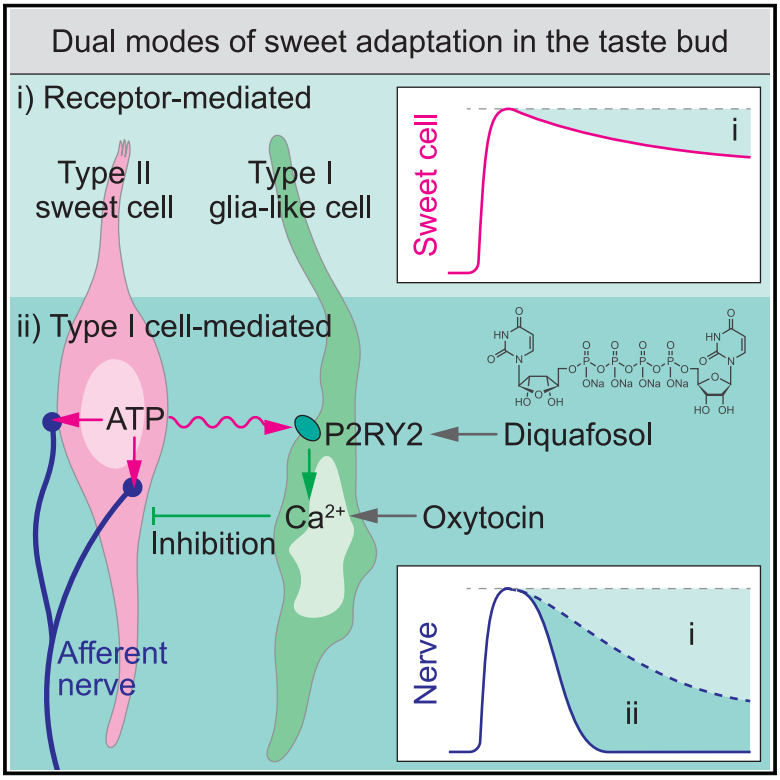

Highlights

- Sweet adaptation is facilitated during synaptic transduction in the taste bud
- ATP from type II cells triggers prolonged responses in adjacent type I cells via P2RY2
- Purinergic activation of type I cells provides inhibitory modulation to sweet taste
- A clinically approved P2RY2 agonist, diquafosol, attenuates sweet perception

Authors

Gha Yeon Park, Geehyun Lee, Jongmin Yoon, ..., Zhaofa Wu, Yulong Li, Myunghwan Choi

Correspondence

choim@snu.ac.kr

In brief

Intercellular crosstalk between glia-like type I and chemosensory type II cells provides an alternative mode of sweet adaptation on the tongue.

Park et al., 2025, Cell *188*, 1–16
January 9, 2025 © 2024 Elsevier Inc. All rights are reserved, including those for text and data mining, AI training, and similar technologies.
https://doi.org/10.1016/j.cell.2024.10.041

CellPress

Please cite this article in press as: Park et al., Glia-like taste cells mediate an intercellular mode of peripheral sweet adaptation, Cell (2025), https://doi.org/10.1016/j.cell.2024.10.041

Cell

CellPress

Article

Glia-like taste cells mediate an intercellular mode of peripheral sweet adaptation

Gha Yeon Park,[1,2,5] Geehyun Lee,[1,2,5] Jongmin Yoon,[1,2] Jisoo Han,[3] Pyonggang Choi,[3] Minjae Kim,[1,2] Sungho Lee,[1,2] Chaeri Park,[1,2] Zhaofa Wu,[4] Yulong Li,[4] and Myunghwan Choi[1,2,6,*]

[1]School of Biological Sciences, Seoul National University, Seoul 08826, Republic of Korea
[2]The Institute of Molecular Biology and Genetics, Seoul 08826, Republic of Korea
[3]Korea Brain Research Institute, Daegu 41062, Republic of Korea
[4]State Key Laboratory of Membrane Biology, Peking University School of Life Sciences, Beijing 100871, China
[5]These authors contributed equally
[6]Lead contact
*Correspondence: choim@snu.ac.kr
https://doi.org/10.1016/j.cell.2024.10.041

SUMMARY

The sense of taste generally shows diminishing sensitivity to prolonged sweet stimuli, referred to as sweet adaptation. Yet, its mechanistic landscape remains incomplete. Here, we report that glia-like type I cells provide a distinct mode of sweet adaptation via intercellular crosstalk with chemosensory type II cells. Using the microfluidic-based intravital tongue imaging system, we found that sweet adaptation is facilitated along the synaptic transduction from type II cells to gustatory afferent nerves, while type I cells display temporally delayed and prolonged activities. We identified that type I cells receive purinergic input from adjacent type II cells via P2RY2 and provide inhibitory feedback to the synaptic transduction of sweet taste. Aligning with our cellular-level findings, purinergic activation of type I cells attenuated sweet licking behavior, and P2RY2 knockout mice showed decelerated adaptation behavior. Our study highlights a veiled intercellular mode of sweet adaptation, potentially contributing to the efficient encoding of prolonged sweetness.

INTRODUCTION

Sensory systems often show diminishing sensitivity to prolonged or repeated sensory stimuli, a phenomenon known as sensory adaptation.[1,2] Starting from the sensory end organs, sensory adaptation occurs at multiple levels by diverse molecular and cellular mechanisms and contributes to the efficient coding of a wide range of dynamic sensory inputs.[3–6] For example, retinal photoreceptor cells in the visual system undergo photopic adaptation on a millisecond scale to maintain their sensitivity across a wide range of luminance levels.[7] Similarly, olfactory sensory neurons in the nasal epithelium rapidly desensitize when exposed to an odorant over a prolonged period to tune the olfactory sensitivity toward novel odorants in the environment.[8] In the skin, Merkel cells express slowly adapting mechanoreceptors for encoding sustained pressure, while Pacinian corpuscles equip rapidly adapting mechanoreceptors for sensing mechanical vibration.[9,10] These sensory adaptation phenomena are evolutionarily conserved in animals and humans.[11–13]

Likewise, the taste system also displays sensory adaptation. A well-known example is sweet adaptation revealed by psychophysics studies on human subjects, showing that pre-exposure to sweet compounds led to a significant reduction in subsequent perception of sweetness.[14–16] Consistent observations of taste adaptation in gustatory nerve recordings on diverse animal models were reported subsequently.[17,18] Later, the identification of a mammalian sweetener receptor, a heterodimer of T1R2 and T1R3,[19–21] expressed on sweet-sensing cells in various organs,[22] led to the finding that the receptors can be gradually desensitized in response to repeated or prolonged sweet stimuli, mediating sweet adaptation.[23] This receptor-mediated adaptation, conceivably occurring in chemosensory cells in the taste bud, has long been regarded as the primary mechanism of peripheral sweet adaptation.[24–26]

The taste bud comprises not only chemosensory cells (type II for sweet, bitter, and umami; type III for sour) but also glia-like cells (type I), which are the most abundant cell type in the taste bud.[27–34] Despite their abundance, type I cells have long been considered merely as supporters or bystanders in the taste transduction pathway, primarily due to their lack of taste receptors and anatomical connectivity to gustatory afferents.[35,36] Nonetheless, a line of histological and functional studies conducted particularly in the context of bitter and salty stimuli has raised intriguing speculations on their active role in taste information processing.[37–40]

Here, we report a mode of sweet adaptation mediated by intercellular interactions between type II and type I cells. First, we established an optical approach for visualizing individual functional elements in the taste bud *in vivo*, including type II cells, extracellular adenosine triphosphate (ATP) release,

All rights are reserved, including those for text and data mining, AI training, and similar technologies.

Please cite this article in press as: Park et al., Glia-like taste cells mediate an intercellular mode of peripheral sweet adaptation, Cell (2025), https://doi.org/10.1016/j.cell.2024.10.041

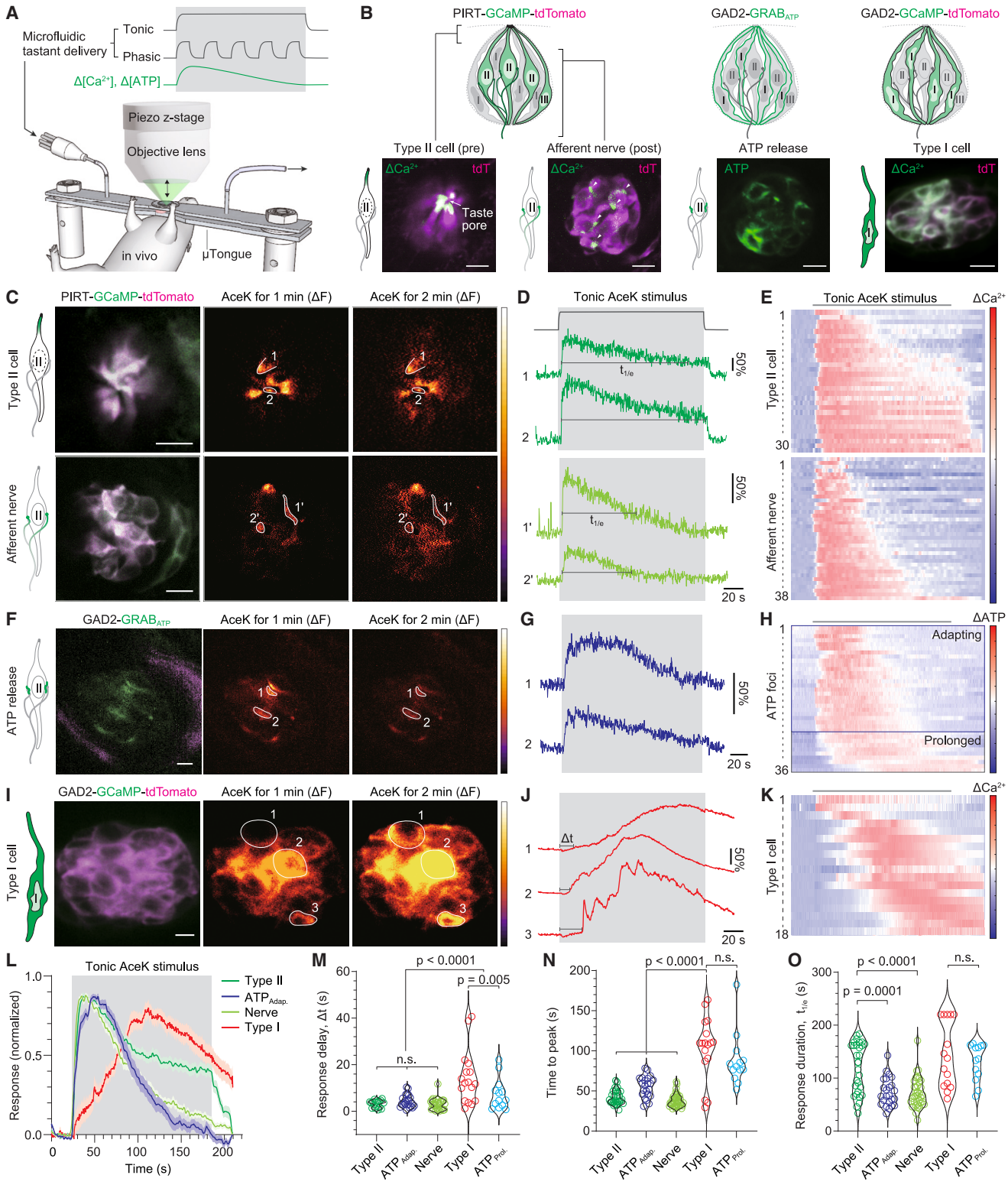

Figure 1. Cellular-subtype-specific functional dynamics within the taste bud during prolonged sweet stimuli *in vivo*

(A) Experimental setup. The μTongue system provides programmable tastant delivery. Functional dynamics within a taste bud is volumetrically recorded using a piezo z-scanning.

(legend continued on next page)

Please cite this article in press as: Park et al., Glia-like taste cells mediate an intercellular mode of peripheral sweet adaptation, Cell (2025), https://doi.org/10.1016/j.cell.2024.10.041

afferent nerves, and type I cells. Second, harnessing the *in vivo* imaging approach, we comprehensively screened their functional activities in the context of sweet adaptation, revealing cellular-subtype-specific functional dynamics in the taste bud. Third, we identified the molecular mediators for the intercellular interactions including the purinergic receptor subtype in type I cells. Moreover, we revealed that functional activation of type I cells provides reliable inhibitory modulation to peripheral sweet information. Finally, we demonstrated that the functional activity of type I cells influences the perception of sweet taste.

RESULTS

Facilitation of sweet adaptation in the taste bud

To investigate peripheral sweet adaptation *in vivo*, we employed the microfluidics-based tongue imaging chamber (μTongue) to cell-type-specific reporter mice with either intracellular calcium or extracellular neurotransmitter sensors[41–44] (Figure 1A). Through the embedded microfluidic channel of the μTongue system, we programmatically delivered a sweet tastant (30 mM acesulfame potassium [AceK]) to the dorsal surface of the tongue in phasic (5 times 10-s exposures with 20-s intervals) or tonic (a single 160-s exposure) stimulus protocols to induce sweet adaptation in a physiological context. To visualize the sweet transduction pathway, we used PIRT-GCaMP-tdTomato mice, which label chemosensory type II and III taste cells, along with their downstream geniculate neurons (Figures 1B and S1). Through real-time volumetric imaging of the taste bud, we concurrently visualized intracellular calcium activities of sweet-responding taste cells and axonal arbors of the afferent nerves in the taste bud. Since our protocol resulted in mostly segregated sweet- and sour-responsive cell populations, we attributed sweet-responsive cells to type II cells (specificity = 94%, n = 16 cells; Figure S1).[42] Although afferent nerves are in close proximity with type II cells to form unconventional synapses,[45] we were able to unambiguously distinguish the sweet-evoked signal of type II cells from that of afferent nerves since they are spatially segregated to the apical and basolateral domains, respectively (Figures 1B, S1G, and S1H). Consistently, after bilateral transection of chorda tympani nerves innervating the fungiform taste buds, the basolateral responses corresponding to the afferent nerves were selectively abolished, whereas the apical type II cell responses remained preserved (Figures S1I–S1K).

Using PIRT-GCaMP-tdTomato mice, we first investigated the synaptic transmission of sweet information from type II cells to afferent nerves during tonic and phasic sweet stimuli. As expected by the known receptor-mediated adaptation, the calcium activities of type II cells showed a gradual decline during phasic and tonic sweet stimulus (Figures 1C–1E and S2; Videos S1 and S2). The response of the downstream afferent nerves also showed a decline; however, their adaptation kinetics notably exceeded that of type II cells in both phasic and tonic stimulus conditions. For example, in response to the tonic stimulus of 160 s, the 1/e response durations ($t_{1/e}$) were significantly decreased from 120.2 ± 8.6 s in type II cells to 71.9 ± 4.7 s in afferent nerves (n = 30 for type II cells and n = 38 for afferent nerves; $p < 0.0001$, unpaired t test; Figure 1O), indicating facilitation of adaptation kinetics. In the phasor diagram representing the functional relationship between type II cells and afferent nerves, both phasic and tonic conditions exhibited apparent facilitated adaptation along a common trajectory (Figure S2M). Moreover, we confirmed that this phenomenon is not only limited to acesulfame K but also in other sweet compounds such as fructose, saccharine, and sucralose, all of which consistently exhibit facilitated adaptation kinetics at the levels of gustatory afferents and geniculate neurons (Figures S2N and S2O). We also observed similar facilitated adaptation at the afferent nerve level with bitter and umami tastants but not with sour and salty tastants, suggesting that the facilitated adaptation is selective to taste qualities transduced by type II cells (Figure S3). This finding of facilitated adaptation from type II cells to afferent nerves implies that an alternative mechanism of sweet adaptation exists within the taste bud, beyond the previously recognized receptor-mediated adaptation.

To visualize the transmitter released from the type II cells,[46,47] we adopted the P2Y1 receptor-based fluorescent sensor, $GRAB_{ATP}$, expressed under the GAD2 promoter[48] (Figure 1B). Owing to the inherent sensitivity of the P2Y1 receptor, $GRAB_{ATP}$ detects both ATP and ADP. However, the ATP transmitter released by type II cells is rapidly hydrolyzed into ADP, AMP, and adenosine and is timely cleared from the extracellular space to ensure temporally defined transduction of taste signal and microenvironmental homeostasis.[49,50] Thus, ADP kinetics largely follow ATP kinetics, and consequently, $GRAB_{ATP}$ recapitulates the dynamics of ATP release by type II cells. The dynamics of ATP release measured by $GRAB_{ATP}$ mice in response to tonic sweet stimuli exhibited the two major kinetic clusters composed

(B) Mouse models. PIRT-GCaMP-tdTomato mouse (left) labels both type II cells and afferent nerves in the taste bud. GAD2-$GRAB_{ATP}$ mouse (middle) visualizes extracellular ATP. GAD2-GCaMP-tdTomato mouse (right) labels glia-like type I cells. Scale bar, 10 μm.
(C) Representative calcium activity in the apical side of type II cells (top) and basolateral afferent nerves (bottom) during a tonic sweet stimulus (AceK 30 mM, 160 s) in a PIRT-GCaMP6-tdTomato mouse. Scale bar, 10 μm.
(D) Representative calcium activities of type II taste cells (dark green) and afferent nerves (light green) in (A). The shaded gray area represents the duration of 30 mM AceK stimulus. $t_{1/e}$ indicates the response duration of which ΔF/F is greater than 1/e (~36.8%) of the maximal response.
(E) Heatmap for type II cells (n = 30 cells) and afferent nerves (n = 38 nerves).
(F–H) Extracellular ATP release in response to tonic sweet stimuli measured in GAD2-$GRAB_{ATP}$ mice. n = 36 synaptic foci from 11 mice in (H). The data in (H) is sorted by the hierarchical clustering analysis. The two major clusters are indicated as adapting (n = 23 foci) and prolonged (n = 13 foci). Scale bar, 10 μm.
(I–K) Type I cell activity in response to tonic sweet stimuli measured in GAD2-GCaMP6f-tdTomato mice. n = 18 cells from 5 mice in (K). Scale bar, 10 μm.
(L) Summarized functional responses of type II cells (dark green), on-time ATP release (purple), afferent nerves (light green), and type I taste cells (red) to tonic sweet stimuli.
(M–O) Quantitative comparison of response delay (Δt), time to peak, and response duration ($t_{1/e}$). One-way ANOVA test.
See also Figures S1, S2, S3, and S4.

Please cite this article in press as: Park et al., Glia-like taste cells mediate an intercellular mode of peripheral sweet adaptation, Cell (2025), https://doi.org/10.1016/j.cell.2024.10.041

of "adapting" and "prolonged" (Figures 1F–1H; n = 23 foci for adapting, n = 13 foci for prolonged by hierarchical clustering analysis). The adapting kinetics showed gradual desensitization with minimal response delays and largely resembled the functional dynamics of afferent nerves rather than that of type II cells, suggesting that facilitated adaptation occurs at the level of type II cells. The prolonged kinetics, however, showed significantly delayed response onsets by 6.0 ± 6.4 s, and the response durations were prolonged compared with the adapting kinetics. Intriguingly, the prolonged kinetics was absent in both type II cells and afferent nerves, implicating that this ATP kinetics might serve a distinct function beyond the conventional synaptic transmission from type II cells to afferent nerves.

Distinct temporal kinetics of type I cells during sweet adaptation

We next studied the functional dynamics of glia-like type I cells during sweet adaptation using GAD2-GCaMP-tdTomato mice[51] (specificity = 74% and sensitivity = 94%; Figures 1B and S1A–S1D; Video S3). Of note, in response to tonic sweet stimuli, type I cells displayed a significantly delayed sweet-evoked response of 18.0 ± 13.8 s (n = 18 cells), which was in stark contrast with the canonical taste transduction pathway from type II cells to afferent nerves responding nearly on time upon the arrival of a stimulus (Figures 1I–1M). The time to peak of type I cells was also distinctively slow compared with the canonical pathway (Figure 1N). The response duration ($t_{1/e}$) of type I cells was prolonged often beyond the cessation of the sweet stimuli (8 out of 18 cells), which was never observed in type II cells and afferent nerves (0 out of 30 cells and 0 out of 38 nerves; Figure 1O). These distinctive kinetic features were consistently observed with other stimulus conditions, such as a phasic sweet stimulus or a single 20-second exposure to other basic taste qualities (Figure S2).[52] The kinetic parameters of type I cells resembled the prolonged kinetics observed in extracellular ATP (Figures 1M–1O), although its causal relationship with type I cells remains to be verified.

The functional distinction between type I and type II cells was also apparent in their stimulus-response relationship (Figure S4). With increasing duration of sweet stimuli (0–30 s of 30 mM AceK), type I cells showed a large supralinear rise in their integrated responses, whereas type II cells showed a moderate sublinear relationship (Figures S4A and S4B). In response to the increasing concentrations of sweet stimuli (0–80 mM AceK), type I cells showed a progressive increase in the number of responding cells, primarily through propagation to neighboring type I cells. By contrast, type II cells showed saturable responses conceivably defined by the expression levels of sweet receptors (Figures S4C and S4D). In agreement with the gradual spreading of type I cell response, a portion of extracellular ATP also showed spatially spreading dynamics during phasic and tonic sweet stimuli, which were classified as prolonged kinetics (Figures S4E–S4H). These distinctive response characteristics of type I cells imply that they are preferentially activated in the context of prolonged or intense taste stimuli.

To summarize, our functional screening revealed that the sweet adaptation kinetics is facilitated along the synaptic transduction at the downstream of taste receptors, suggesting the presence of an alternative adaptation mechanism other than the known receptor-mediated mechanism. Intriguingly, type I cells display delayed and prolonged responses, seemingly negatively correlated with the adapting kinetics. Thus, we subsequently investigated the underlying mechanism of the type I cell response and its functional outcome.

Purinergic signaling from type II to type I cells via P2Y2 receptors

As type I cells do not express any sweet taste receptors, we reasoned that their sweet-evoked responses are mediated by sweet-sensing type II cells. To verify this, we investigated type I cell responses in PLCβ2 knockout mice lacking sweet and bitter reception[53,54] (Figures 2A–2D). Contrary to the wild-type mice showing broad responsiveness to sweet, bitter, and salty stimuli, sweet- and bitter-evoked calcium responses in type I cells were selectively abolished in PLCβ2 knockout mice. This result suggests that sweet-evoked responses of type I cells are mediated by intercellular interactions with sweet-sensing type II cells.

We next questioned if ATP released by type II cells mediates the functional interaction with type I cells. First, we examined sweet-evoked responses of type I cells in the presence of a purinergic receptor inhibitor. After intravenous delivery of suramin, the sweet-evoked type I cell calcium responses were significantly attenuated (Figures 2E and 2F). Second, we observed that type I cells were broadly responsive to intravenously administered ATP (Figures 2G and 2H). Lastly, to determine if sweet-responsive type I cells are positioned adjacent to sweet-sensing type II cells, we conducted correlative imaging by serially performing *in vivo* calcium imaging and post-mortem mRNA *in situ* hybridization (FISH) on the same taste bud. Indeed, in all fungiform taste buds we observed (n = 4 taste buds), the sweet-responsive type I cells in GAD2-GCaMP-tdTomato mice were positioned adjacent to the sweet-sensing type II cells marked by the TAS1R2 probe (Figures 2I–2K). These results collectively indicate that ATP released by type II cells is the major paracrine mediator for the sweet-evoked responses of type I cells.

In order to identify the specific receptor subtype responsible for the purinergic signaling from type II to type I cells, we screened a panel of purinergic agonists on type I cells *in vivo* (Figure 3). In our initial screening with ATP, adenosine diphosphate (ADP), uridine triphosphate (UTP), uridine diphosphate (UDP), 3′-O-(4-benzoylbenzoyl) ATP (BzATP), and ATP-gamma-S (ATPγS), only ATPγS, the non-hydrolyzable analog of ATP, was shown to be effective when topically applied on the tongue (Figure 3A), conceivably due to the high level of ATPase within the taste bud (e.g., ENTPDase in type I cells).[49] Thus, we carried out the next screening with hydrolysis-resistant analogs, including ATPγS (P2 receptor agonist), UTPγS (P2RY2 and P2RY4 agonist), diquafosol (P2RY2 agonist), and 2-MeSATP (P2X receptors, P2RY1, P2RY6, P2Y11, and P2Y13 agonist).[55–61] We found that ATPγS, UTPγS, and diquafosol were potent stimuli when topically applied on the tongue (Figures 3B and 3C; Video S4). Based on the receptor subtype specificities of these ligands, we identified the P2Y2 receptor as the primary functional receptor in type I cells. Diquafosol primarily activated the apical side of type I cells, and the dose-response relationship measured *in vivo* yielded an EC_{50} value

Please cite this article in press as: Park et al., Glia-like taste cells mediate an intercellular mode of peripheral sweet adaptation, Cell (2025), https://doi.org/10.1016/j.cell.2024.10.041

CellPress

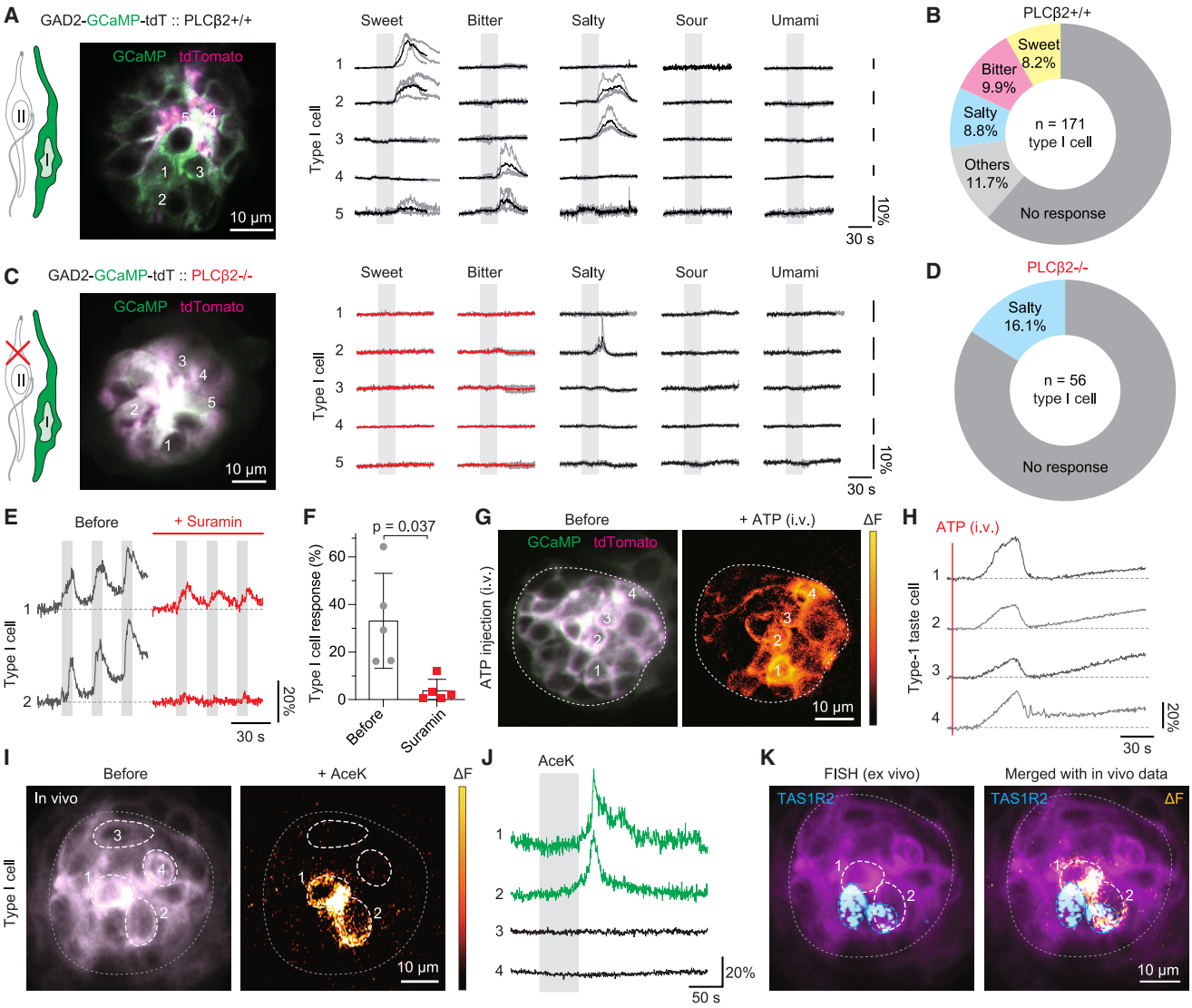

Figure 2. Sweet-evoked calcium response of type I cells is mediated by ATP released from type II cells

(A–D) Functional responses of type I cells to five basic tastes in GAD2-GCaMP5g-tdTomato mice (n = 171 cells for PLCβ2+/+ and n = 56 cells for PLCβ2−/−). Gray curves indicate individual trials (n = 3) and the dark curves indicate the averaged traces.

(E and F) Inhibition of purinergic receptors. Intravenous delivery of 1 mM suramin led to attenuation of type I cell responsiveness to sweet stimuli (30 mM AceK, shaded in gray). p = 0.037 by paired t test.

(G and H) Functional responses of type I cells to ATP. ATP (5 mM, 100 μL) was intravenously injected using a retro-orbital catheter.

(I–K) Correlative *in vivo-ex vivo* imaging. Sweet-evoked functional responses (30 mM AceK) of type I cells were recorded in (I) and (J), and subsequently the same taste bud underwent FISH with TAS1R2 probe in (K).

of ~407 μM, which was several orders of magnitude higher than the EC_{50} value reported *in vitro*, likely due to the tight junction barriers at the apical pore[62] (Figures 3D–3F). The calcium activities of diquafosol-responsive type I cells were inhibited by mucosal delivery of P2RY2 selective antagonist, AR-C 118925[63] (Figures 3G and 3H). Additionally, we confirmed that diquafosol did not evoke any notable calcium responses in sweet-responsive type II cells or sour-responsive type III cells (Figures S5A and S5B). Among the topically potent candidates, we chose diquafosol for the following studies since it has excellent specificity to P2RY2 and is clinically approved for use as an ophthalmic solution.[64]

Next, to verify the presence of P2RY2 in type I cells, we performed multiplexed FISH in fungiform taste buds with six mRNA probes, including P2RY2 and cell-type markers (type I cell: ENTPDase2 and GAD2; type II sweet cell: TAS1R2 and TAS1R3, type III cell: CAR4). Given the morphological complexity of type I cells with their lamellar processes enwrapping other taste cells, we only counted P2RY2 signals located within the nuclei demarcated by DAPI labeling. We observed

Please cite this article in press as: Park et al., Glia-like taste cells mediate an intercellular mode of peripheral sweet adaptation, Cell (2025), https://doi.org/10.1016/j.cell.2024.10.041

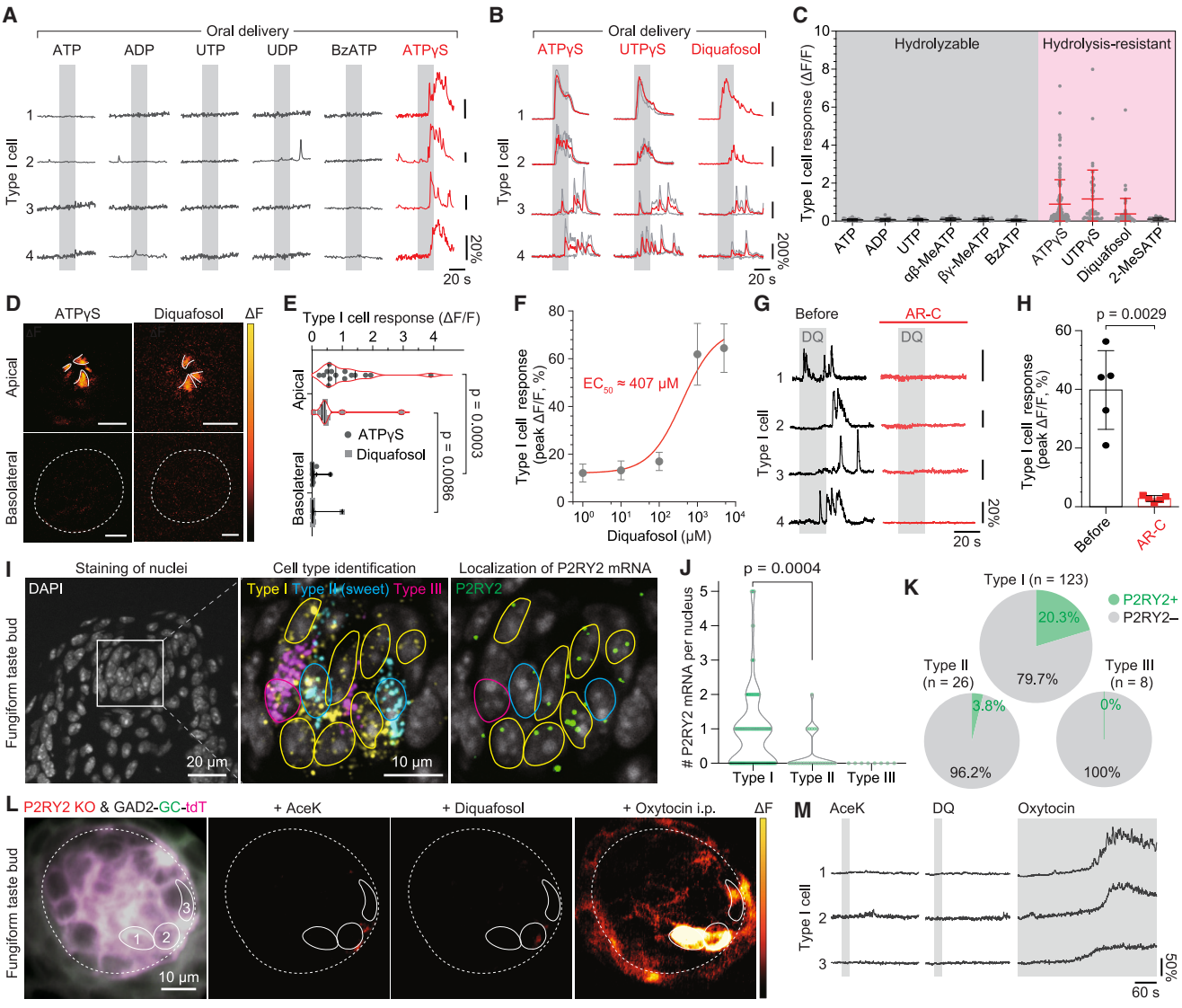

Figure 3. P2RY2 mediates the purinergic signaling from type II to type I cells

(A–C) Calcium responses of type I cells to topically delivered purinergic agonists (n = 4 cells each). Only the non-hydrolyzable analogs (150 μM ATPγS, 150 μM UTPγS, and 1 mM diquafosol) with P2RY2 sensitivity evoked robust responses.

(D and E) Spatial profile of type I cell response to topically delivered non-hydrolyzable ATP analogs. The response was predominantly observed only on the apical side. Scale bar, 10 μm.

(F) Dose-response relationship of the type I cell activity at the apical pore to diquafosol.

(G and H) Pharmacological inhibition of P2RY2. Submucosal injection of AR-C 118925 (10 μM, ~4 μL) abolished the type I cell response to 5 mM diquafosol (n = 5 cells). p = 0.0029 by paired t test.

(I) Multiplexed FISH data on cell-type markers and P2RY2. Cell-type markers: GAD2 and NTPDase2 for type I cells, TAS1R2 for sweet-sensing type II cells, and CAR4 for type III cells.

(J and K) Quantitative analyses of P2RY2 transcripts for each cell type. A cell was classified as P2RY2-positive if it contained two or more P2RY2 transcripts within its nucleus. p = 0.0004 by Mann-Whitney unpaired t test (n = 157 cells from 2 mice).

(L and M) Calcium responses in type I cells in response to diquafosol (5 mM, 20 s), AceK (30 mM, 20 s), and intraperitoneal oxytocin (0.1 mg/kg) in a P2RY2−/−; GAD2-GCaMP mouse.

See also Figure S5.

that P2RY2 transcripts were predominantly distributed within the type I cells (Figure 3I). By contrast, P2RY4, the alternative target of diquafosol with compromised sensitivity,[59] was rarely observed within the fungiform taste buds (Figures S5C and S5D). Considering the limited selectivity of the P2RY2 probe, we conservatively defined P2RY2-positive taste cells as cells possessing two or more P2RY2 transcripts within their nuclei (Figures S5E and S5F). The resulting P2RY2-positive cells were

Please cite this article in press as: Park et al., Glia-like taste cells mediate an intercellular mode of peripheral sweet adaptation, Cell (2025), https://doi.org/10.1016/j.cell.2024.10.041

20.3% for type I cells (n = 126 type I cells), 3.8% for type II sweet cells (n = 26 cells), and 0% for type III cells (n = 8 cells; Figures 3J and 3K). Immunohistochemistry consistently supported the expression of P2RY2 proteins in the fungiform taste buds (Figure S5G). Analysis of spatial distribution among cell types using the multiplexed FISH data showed that the TAS1R2/3-positive sweet cells were preferentially positioned close to the P2RY2-positive type I cells compared with other cell types, suggesting taste modality-specific influence of type I cells (Figures S5H–S5K). Additionally, we confirmed that the P2RY2 transcript is negligible in geniculate neurons innervating the fungiform taste buds by performing mRNA FISH on the isolated geniculate ganglion (Figures S5L and S5M) and by reanalyzing the published transcriptome data from Dvoryanchikov et al.[65] (Figures S5N and S5O).

Finally, we investigated if P2RY2 is necessary for sweet-evoked type I cell responses employing the P2RY2 knockout model. To observe the functional responsiveness of type I cells in the P2RY2 knockout model, we generated P2RY2−/−; GAD2-GCaMP mice by crossbreeding the P2RY2 knockout line with GAD2-cre and flex-GCaMP reporter lines (Figure 3L). In stark contrast to the wild-type control, type I cells in P2RY2 knockout mice lost their responsiveness to AceK and diquafosol, suggesting that P2RY2 is the major receptor subtype mediating the purinergic crosstalk with type II cells (Figures 3L and 3M). Oxytocin-evoked type I cell responses, mediated independently by the oxytocin receptors, remained intact.[66]

In short, our functional screening, pharmacological and genetic interventions, and mRNA imaging results unanimously point to P2RY2 as the purinergic receptor subtype mediating purinergic signaling from type II to type I cells.

Inhibitory modulation of sweet taste information by type I cells

Given that sweet adaptation is facilitated over time and type I cells show prolonged functional activities by receiving purinergic inputs from type II cells, we hypothesized that type I cells may offer inhibitory feedback as a result of their activation to mediate facilitated sweet adaptation. To investigate the functional consequence of purinergic activation of type I cells, we examined the effects of synthetic activation or deactivation of these cells on peripheral sweet information transduction.

First, we pre-exposed diquafosol on the tongue dorsum for a duration of 15 s to induce purinergic activation of type I cells and quantified ATP release of type II cells and calcium activity of afferent nerves in response to sweet stimuli (Figures 4A–4F). The inter-trial interval with artificial saliva washout was set to >5 min to avoid any potential influence of prior trials. In control trials with pre-exposure of artificial saliva, we did not observe any trial-by-trial differences in sweet-evoked ATP releases (p = 0.396 by Wilcoxon paired t test) or nerve activities (p = 0.082 by Wilcoxon paired t test), indicating non-significant inter-trial influence in our protocol (Figures S6A–S6D). By contrast, pre-exposure to diquafosol resulted in significant reductions of sweet-evoked ATP releases by ∼43% (AUC, p < 0.0001 by Wilcoxon paired t test) and sweet-evoked nerve activities by ∼18% (AUC, p = 0.002 by Wilcoxon paired t test; Figures 4A–4F and S6E–S6I). The sweet inhibitory effect of diquafosol was abrogated in P2RY2 knockout mice (Figures S6J and S6K). In other taste modalities, the pre-activation of type I cells via diquafosol resulted in a taste modality-specific influence. The bitter responses exhibited a significant reduction akin to the impact observed in sweet-responsive nerves, whereas the sour- and salty-responsive nerves remained unaffected (Figures S6L–S6W). Although statistically non-significant, umami-responsive nerves also displayed a moderate decrease.

Second, based on the prior histological report on the oxytocin receptor specifically expressed in type I cells,[66] we used oxytocin to induce specific functional activation of type I cells bypassing the purinergic signaling. In GAD2-GCaMP-tdTomato mice, we confirmed that oxytocin administration via an intraperitoneal catheter robustly induced intracellular calcium activities in type I cells over several minutes (Figure 4G). Following oxytocin administration, sweet-evoked ATP releases in GAD2-GRAB$_{ATP}$ mice and afferent nerve responses in PIRT-GCaMP-tdTomato mice were significantly attenuated by ∼39% and ∼36%, respectively (p < 0.0001 by Wilcoxon paired t test; Figures 4H–4N; Video S5). We estimate that the stronger type I cell activation by oxytocin compared with diquafosol resulted in a more pronounced inhibition of peripheral sweet information. This result aligns with a previous behavior study demonstrating decreased sweet preference in mice pre-injected with oxytocin.[67]

Third, to decouple the purinergic interaction between type II and type I cells, we introduced P2RY2 knockout mice and genetically labeled their afferent nerves through intravenous delivery of AAV-PHP.S::GCaMP6f[68] (Figure 5A). We measured afferent nerve activities in response to tonic sweet stimuli in both wild-type control and P2RY2 knockout mice. Individual afferent nerves in both groups showed diverse adaptation kinetics, at least in part due to the heterogeneity in durations of receptor-level adaptation (Figures 5B–5D). Thus, we sorted the data with respect to the response duration ($t_{1/e}$) and statistically compared the group differences in probability distributions. Notably, P2RY2 knockout mice (n = 57 nerves in 5 mice) showed more prolonged response durations ($t_{1/e}$), compared with the wild-type control group (n = 50 nerves in 7 mice) in their cumulative distribution functions (p = 0.034, unpaired t test). Other kinetic parameters, such as response delay and time to peak, did not show significant differences (Figures 5E–5H). Interestingly, the probability density function of the response duration in wild-type mice showed a bi-gaussian distribution composed of ∼32% of rapidly adapting ($t_{1/e}$ < 41.2 s) and ∼68% of slowly adapting ($t_{1/e}$ > 41.2 s) subgroups (Figures 5I–5L). By contrast, the probability density function in P2RY2 knockout mice showed a unimodal gaussian distribution, predominantly consisting of the slowly adapting subgroup. Our pharmacological activation and genetic inactivation results collectively suggest that the purinergic input to type I cells via P2RY2 receptors facilitates peripheral sweet adaptation, leading to generate afferent nerves with more rapidly adapting kinetics.

Additionally, we performed a computational decoding study to evaluate the functional consequences of the distinct kinetics in nerve responses mediated by P2RY2. To address this, we trained the hidden neural network (HNN) decoder to predict the duration of taste stimuli using the experimentally measured durations of nerve responses as input and compared the decoding

Please cite this article in press as: Park et al., Glia-like taste cells mediate an intercellular mode of peripheral sweet adaptation, Cell (2025), https://doi.org/10.1016/j.cell.2024.10.041

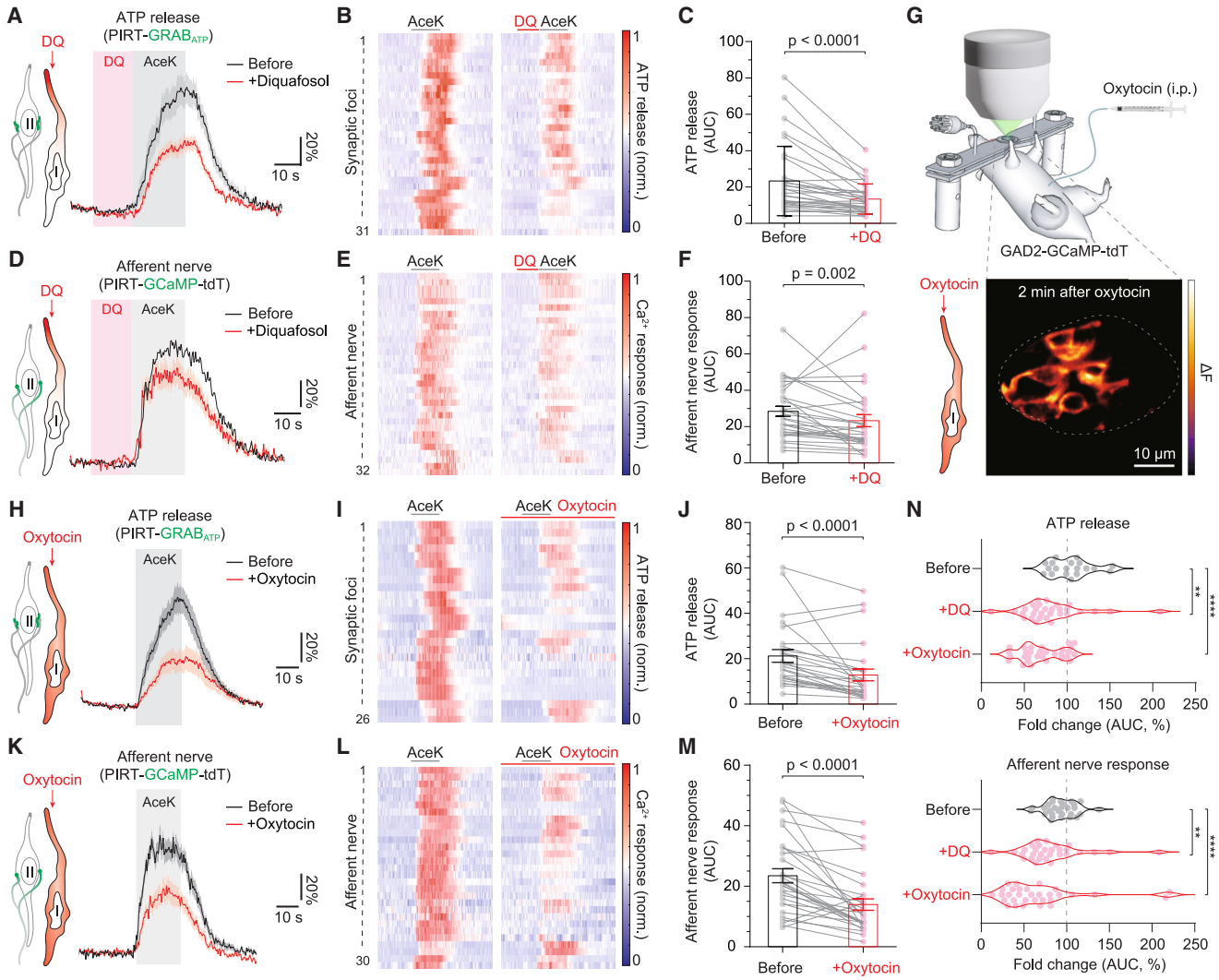

Figure 4. Functional activation of type I cells provides inhibitory modulation to peripheral transduction of sweet taste

(A–C) Inhibitory modulation of sweet-evoked ATP release by diquafosol. Before traces in gray were acquired with exposure to 30 mM AceK for 20 s in PIRT-GRAB$_{ATP}$ mice. Diquafosol traces in red were acquired with pre-exposure to 5 mM diquafosol for 15 s (pink), followed by exposure to 30 mM AceK for 20 s (n = 31 foci from 11 mice). $p < 0.0001$ by paired t test in (C).

(D–F) Inhibitory modulation of sweet-evoked nerve response by diquafosol. Using the same stimulus protocol used in (A)–(C), the afferent nerve activity was measured in PIRT-GCaMP-tdTomato mice (n = 32 nerves from 6 mice). $p = 0.002$ by paired t test in (F).

(G) Experimental setup for observing type I cell response during oxytocin administration via an intraperitoneal catheter.

(H–J) Inhibitory modulation of sweet-evoked ATP release by oxytocin. Before traces in gray were acquired with exposure to 30 mM AceK for 20 s in PIRT-GRAB$_{ATP}$ mice. Oxytocin traces in red were acquired at least 1 min after intraperitoneal administration of oxytocin (n = 26 foci from 7 mice). $p < 0.0001$ by paired t test in (J).

(K–M) Inhibitory modulation of sweet-evoked nerve response by oxytocin. Using the same stimulus protocol used in (H)–(J), the afferent nerve activity was measured in PIRT-GCaMP-tdTomato mice (n = 30 nerves from 7 mice). $p < 0.0001$ by paired t test in (M).

(N) Summary of the data in (A)–(M). $^{**}p < 0.01$, $^{****}p < 0.0001$ by ordinary one-way ANOVA test.

See also Figure S6.

performance at varying stimulus durations for the wild-type and P2RY2 knockout mice (Figure 5M). Contrary to the HNN decoder trained with the wild-type data, the decoder trained with P2RY2 knockout data exhibited a selectively impaired ability to predict the durations of shorter stimuli (< 60 s), conceivably attributed to the loss of rapidly adapting nerves (Figure 5N). Consistently, comparison of the Shannon entropy between wild-type and P2RY2 knockout groups resulted in higher entropy in the P2RY2 knockout group, signifying the heightened unpredictability or randomness of the provided durations (Figure 5O). These results imply that the functional interaction between type II and type I cells via P2RY2 contributes to efficiently encoding a broader range of kinetic information in the context of prolonged sweet stimuli.

Please cite this article in press as: Park et al., Glia-like taste cells mediate an intercellular mode of peripheral sweet adaptation, Cell (2025), https://doi.org/10.1016/j.cell.2024.10.041

CellPress

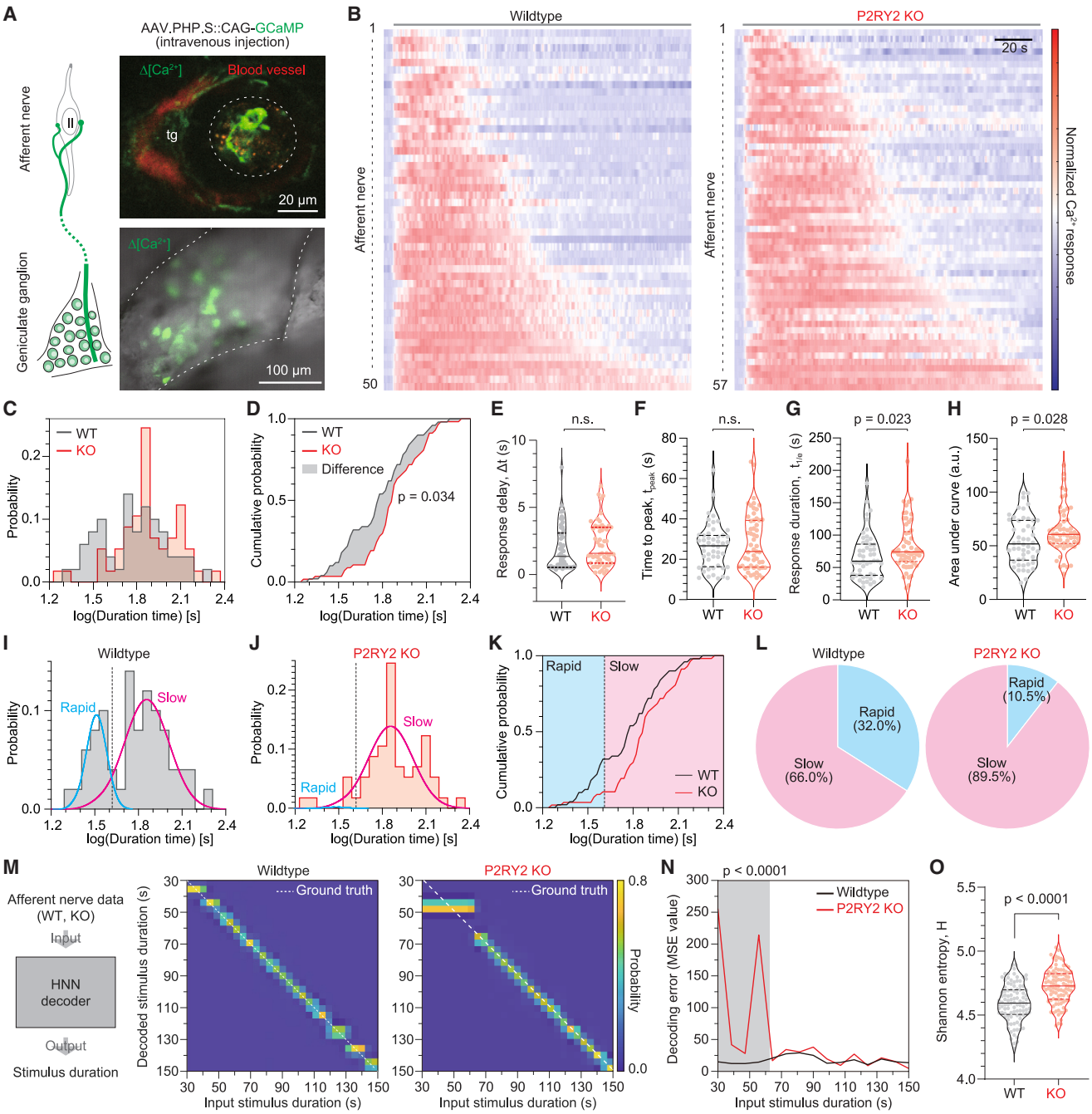

Figure 5. P2RY2 knockout leads to decelerated sweet adaptation

(A) Viral labeling of geniculate neurons and their afferent nerve fibers via intravenous administration of AAV.PHP.S::CAG-GCaMP6. Functional calcium responses (ΔF) of afferent nerves and somas in the geniculate ganglion were acquired in response to the exposure to 30 mM AceK. tg, trigeminal nerves.

(B) Functional responses of afferent nerves during tonic sweet stimuli in wild-type (left, $n = 50$ nerves in 7 mice) and P2RY2 KO mice (right, $n = 57$ nerves in 5 mice). Data are sorted by the response duration ($t_{1/e}$) in ascending order.

(C and D) Probability density and cumulative distribution functions with respect to the response duration ($t_{1/e}$) in log scale. WT, wild-type mice (gray). KO, P2RY2 KO mice (red). $p = 0.034$ by Kolmogorov-Smirnov test.

(E–H) Inter-group comparison of kinetic parameters including response delay (E), time to peak (F), response duration (G), and area under curve (H). $p = 0.255$ in (E), $p = 0.605$ in (F), $p = 0.023$ in (G), and $p = 0.028$ in (H) by Mann-Whitney unpaired t test.

(I and J) Histogram of the response duration of afferent nerves ($t_{1/e}$) under tonic sweet stimuli ($n = 50$ nerves for wild-type and $n = 57$ nerves for KO). The distributions are fitted to the bi-gaussian model (mean: "rapid" = 32.0 s and "slow" = 72.3 s). The dashed line at "$t_{1/e}$ = 41.7 s" indicates the threshold.

(K) Cumulative density function for the duration time ($t_{1/e}$) in wild-type and P2RY2 KO mice.

(legend continued on next page)

Please cite this article in press as: Park et al., Glia-like taste cells mediate an intercellular mode of peripheral sweet adaptation, Cell (2025), https://doi.org/10.1016/j.cell.2024.10.041

Perceptual influence of type I cells

Given the modulatory role of type I cells in peripheral sweet information, we questioned whether the activation of type I cells could also affect sweet perception. To this end, we first conducted a mouse behavior study using the Davis Rig lickometer to measure the influence of diquafosol-elicited type I cell activation on sweet licking behavior. Water-deprived mice of either wild-type or P2RY2 knockout were blindly pre-exposed to either 0.85% saline or 38 mM diquafosol and were subsequently given brief access to a randomized sequence of 0, 10, 20, or 30 mM AceK for 5 s (Figures 6A and 6B; refer to STAR Methods for details). The number of licks during each brief access was recorded to obtain the averaged dose-response curves with and without pre-exposure to diquafosol. In both wild-type and P2RY2 knockout mice, diquafosol did not affect the licking behavior for water as shown in the saline control (Figures 6C–6F). However, pre-exposure to diquafosol significantly suppressed the following sweet licking behavior by ~15% ($p < 0.0001$), which is consistent with our prior observations in the taste bud (Figure 4N). Such an inhibitory effect of diquafosol in sweet licking behavior was not observed in P2RY2 knockout mice (Figures 6E and 6F). These results indicate that P2RY2-mediated activation of type I cells provides inhibitory modulation to sweet perception.

Finally, we investigated the impact of P2RY2-mediated intercellular crosstalk on sweet adaptation behavior (Figures 6G–6J). To quantify behavioral sweet adaptation, we preconditioned water-deprived wild-type or P2RY2 knockout mice by exposing them to 0, 10, 20, or 30 mM AceK in a randomized sequence using the Davis Rig lickometer (Figure 6G). Each trial consisted of a 5-s access to the bottle with an inter-trial interval of 10 s. For initial trials, the water-deprived mice typically exhibited near-maximal licking behavior regardless of AceK concentrations, indicative of binge drinking behavior driven primarily by thirst. However, typically within 25 trials, their licking behavior transitioned to exhibit a preference for sweeter solutions over water.

Once preconditioned to exhibit a higher number of licks toward sweeter solutions, we proceeded to the subsequent session for quantifying sweet adaptation behavior involving 15 consecutive trials of repeatedly exposing them to either 10, 20, or 30 mM AceK (Figure 6G). Reminiscent of peripheral sweet adaptation, wild-type mice showed a gradual decline in the lick rate over trials in a concentration-dependent manner, with sweeter solutions leading to more accelerated adapting kinetics (Figure 6H–6J). To validate if this decline in lick rate is driven by sweet adaptation rather than quenching of thirst, we repeated the sweet adaptation session with a 2-min interval. In the second session, near-maximal lick rates re-emerged in the first trial, and similar adapting kinetics were observed (Figures 6K–6M). These observations suggest that the decline in lick rate during the consecutive AceK trials was primarily driven by sweet adaptation rather than quenching of thirst.

Although P2RY2 knockout mice also showed robust behavioral sweet adaptation, presumably due to the intact other modes of adaptation (e.g., receptor-level adaptation), their adaptation kinetics were significantly slower compared with those observed in wild-type mice (Figures 6H–6J). The most pronounced difference was observed at 30 mM AceK, exhibiting over two-fold slower adaptation kinetics compared with the wild-type control. The stronger influence of P2RY2 knockout at higher concentrations agrees well with our functional imaging data showing that type I cells are preferentially activated at higher concentrations (Figures S4C and S4D). Functionally activated type I cells at higher concentrations would facilitate sweet adaptation only in wild-type mice, resulting in significantly faster adaptation kinetics compared with knockout mice. These results indicate that purinergic crosstalk from type II to type I cells modulates sweet licking behavior in the context of prolonged exposure to intense sweet stimuli.

DISCUSSION

Exploiting our microfluidics-integrated intravital tongue imaging system,[41,42] we unveiled the intercellular mode of peripheral sweet adaptation mediated by the functional crosstalk between glia-like type I cells and chemosensory type II cells. We revealed the purinergic signaling mechanism from synaptic ATP release in type II cells to P2Y2 receptors in type I cells, leading to inhibitory modulation of peripheral sweet information. We further demonstrated at the behavioral level that oral exposure to a clinically applicable P2RY2 agonist, diquafosol, decreases sweet licking behavior, and P2RY2 knockout led to decelerated sweet adaptation. Contrary to the traditional perception of glia-like type I cells as supporting cells,[27,49,69,70] our findings provide direct experimental evidence that these cells can actively exert inhibitory modulation on the peripheral transduction of taste information in a taste modality-specific manner (i.e., sweet and bitter). Conversely, our work aligns well with the report by Rodriguez et al. introducing the concept of tripartite synapse in the taste bud by revealing purinergic signaling from bitter-sensing type II cells to type I cells.[38] Considering the abundance and diversity of type I cells,[39] we believe that there are numerous yet-veiled functional roles of them in taste information processing.

Our study revealed that extracellular ATP released from type II cells can trigger calcium response in type I cells through P2RY2, and the functionally activated type I cells provide negative feedback to type II cells. However, the molecular mediator of the feedback regulation by type I cells remains to be identified. One compelling hypothesis is GABAergic signaling, the major inhibitory neurotransmitter in the nervous system. Type I cells possess GABA synthesized by GAD65, and type II cells express GABA receptors.[71,72] Although type I cells lack synaptic vesicles,[33] non-vesicular release mechanisms—presumably mediated by GABA transporters and channels (e.g., GAT and

(L) Pie charts on rapid- and slow-adapting afferent nerves.
(M) Confusion matrices representing the performance of the HNN decoder trained with the duration data shown in (B). The dotted diagonal lines indicate the ground truth.
(N) The mean squared error of each trained decoder. $p < 0.0001$ by unpaired t test.
(O) Shannon entropy of each group's duration data. Smaller Shannon entropy indicates a more informative dataset. $p < 0.0001$ by unpaired t test.

Please cite this article in press as: Park et al., Glia-like taste cells mediate an intercellular mode of peripheral sweet adaptation, Cell (2025), https://doi.org/10.1016/j.cell.2024.10.041

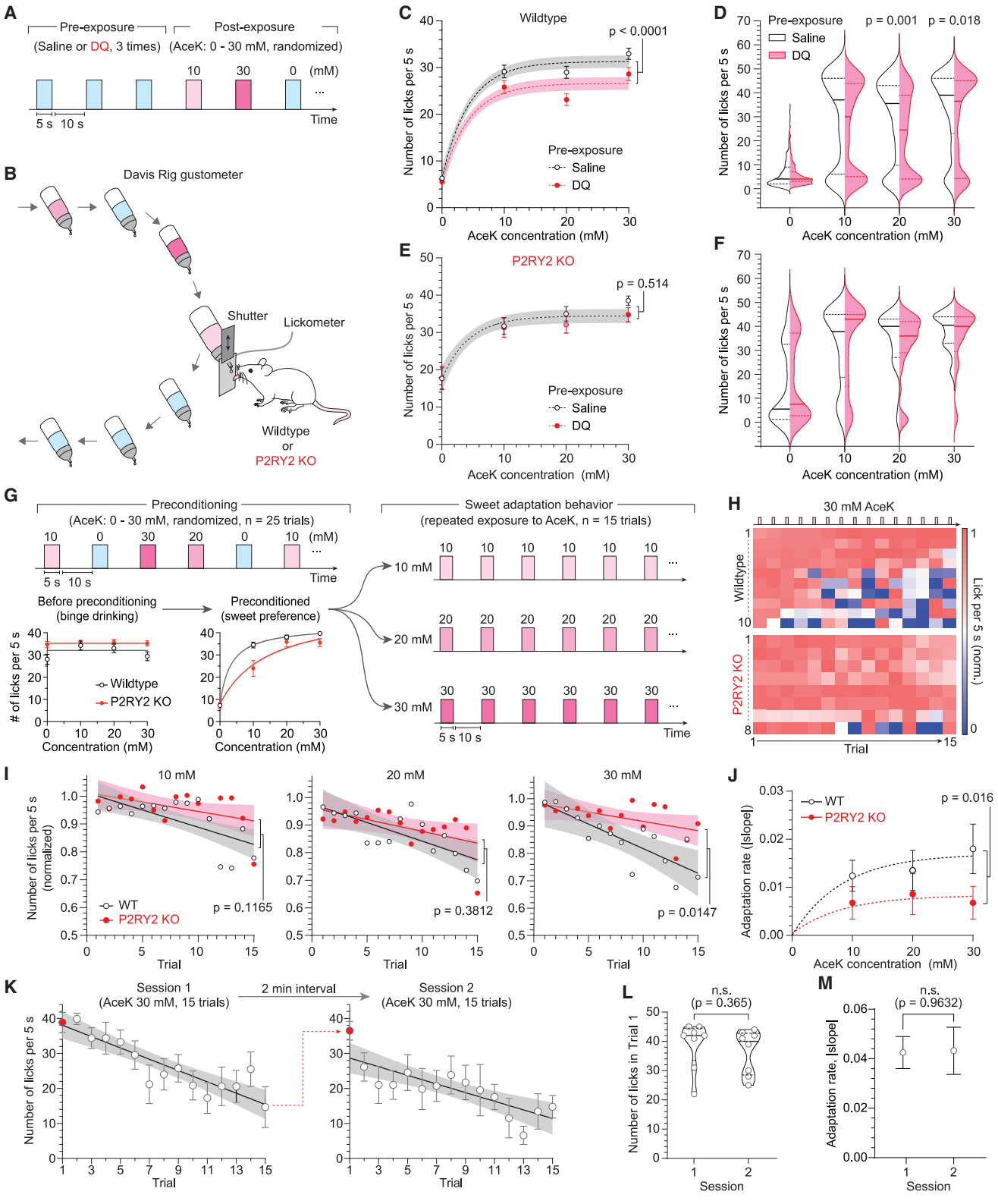

(legend on next page)

Please cite this article in press as: Park et al., Glia-like taste cells mediate an intercellular mode of peripheral sweet adaptation, Cell (2025), https://doi.org/10.1016/j.cell.2024.10.041

Bestrophin-1)—may contribute to the GABA release as reported in astrocytes in the brain.[73,74] Moreover, the potential involvement of type III cells should not be ruled out. Type III cells express P2Y receptors and release serotonin in an activity-dependent manner, which may provide inhibitory modulation to sweet-sensing type II cells.[75,76] Further investigation is required to identify the molecular mediator and its downstream pathway leading to the inhibitory modulation of sweetness.

The origin of the delayed onset observed in type I cells warrants further investigation. The release of ATP by type II cells at the synapse is an immediate process, considering no notable delay in postsynaptic responses of the afferent nerve arbors. Meanwhile, type I cell responses triggered by the ATP released by type II cells showed significant delays of 18.0 ± 13.8 s (Figure 1M). This temporal discrepancy may be explained by the distinct kinetics observed in extracellular ATP signals composed of adapting and prolonged responses. The majority of ATP foci classified as adapting exhibited minimal response delay and gradually desensitizing kinetics comparable to calcium responses in the afferent nerves (Figures 1E and 1H). On the other hand, the remaining ATP foci classified as prolonged displayed notably delayed and prolonged kinetics similar to the calcium responses of type I cells (Figures 1H and 1K). We estimate that these delayed and prolonged kinetics may arise from the extra-synaptic ATP spillover, which may serve as the temporally delayed and spatially extended purinergic input to the adjacent type I cells. In agreement with our conjecture, we observed spatially diffusing ATP signals in response to both phasic and tonic sweet stimuli conditions (Figures S4G and S4H). In parallel, the slow kinetics of metabotropic P2Y2 receptors would, at least in part, contribute to the delayed response.[77,78] Alternatively, hydrolyzed forms of ATP, such as ADP or adenosine, may also contribute to the delayed onset or prolonged response duration.

Efficient encoding of massive sensory inputs from the external world is a hallmark of sensory systems.[79,80] To be computationally 'efficient', the sensory system is required to dynamically tune its sensitivity to match the statistical distribution of external inputs.[81] Thus, sensory adaptation—decreasing the allocation of neural resources to the relatively static input over time—is considered an efficient coding strategy. External inputs, however, vary over a wide range of timescales from milliseconds to minutes, necessitating various molecular and cellular machinery for sensory adaptation.[8,82,83] In this regard, the generation of rapid and slow adaptation kinetics through the receptor- and type I cell-mediated mechanisms aligns well with the concept of efficient coding, enabling encoding of a wider range of timescales observed in physiological ingestive behaviors, spanning from seconds to minutes. Conversely, the loss of rapidly adapting kinetics observed in P2RY2 knockout mice would compromise the efficient coding of prolonged input stimuli. Indeed, our computational study demonstrated that the rapidly adapting nerve signals mediated by type I cells contribute to decoding the stimulus duration for short timescale. To conclude, the rapidly adapting kinetics mediated by type I cells contribute to the efficient encoding of shorter timescales, thereby enhancing the ability to encode temporal information across a wider range of durations.[84]

Our multiplexed mRNA imaging, as well as diquafosol-evoked type I cell activity, indicated that not all but a subset of type I cells possess P2Y2 receptors. Consistently, our functional imaging study on knockout mice demonstrated that P2RY2 is primarily responsible for generating rapidly adapting kinetics, constituting approximately 30% of afferent nerves. These findings also align with our correlative *in vivo-ex vivo* imaging result, showing that sweet-evoked responses of type I cells were spatially confined near the sweet-sensing type II cells. Since a certain level of facilitated adaptation was globally observed from type II cells to afferent nerves, we anticipate the existence of alternative adapting mechanisms, which require further investigation. Additionally, we observed that bitter-sensing type II cells also receive inhibitory modulation from the same purinergic crosstalk, suggesting that intercellular crosstalk between type I and type II cells may also contribute to cross-adaptation or mixture discrimination between sweet and bitter taste qualities.[38,85]

Limitations of the study

First, while our study focused on the sensory adaptation of sweet taste using several types of sweet compounds (Figures S2N and S2O), it is important to acknowledge that other sweet compounds may not exhibit identical results. Previous

Figure 6. Functional activity of type I cells influences perceived sweetness

(A and B) Experimental design for evaluating the effect of functionally activated type 1 cells on sweet licking behavior. Each mouse is blindly exposed to either saline or diquafosol ("pre-exposure") prior to the exposure to a "test" solution containing either 0, 10, 20, or 30 mM AceK in a randomized order using the Davis Rig lickometer ($n = 25$ trials). The lickometer counts licks for the duration of 5 s after the initial lick. The shutter limits the duration of licking to 5 s. DQ, diquafosol.

(C) Dose-response curves of AceK concentration versus lick rate in wild-type mice. $p < 0.0001$ by unpaired t test.

(D) Inter-group comparison of lick rates for each AceK concentration in wild-type mice (saline versus DQ). Solid and dotted lines in violin plots indicate medians and quartiles, respectively. $p = 0.127$ in 0 mM, $p = 0.087$ in 10 mM, $p = 0.001$ in 20 mM, $p = 0.019$ in 30 mM by unpaired t test.

(E) Dose-response curves of AceK concentration versus lick rate in KO mice.

(F) Inter-group comparison of lick rates for each AceK concentration in KO mice (saline versus DQ). $p = 0.776$ in 0 mM, $p = 0.6851$ in 10 mM, $p = 0.125$ in 20 mM, $p = 0.161$ in 30 mM by unpaired t test.

(G) Experimental design for evaluating sweet adaptation behavior. Preconditioning session prior to testing the sweet adaptation behavior.

(H) Heatmap representation of lick rates at 30 mM AceK in wild-type ($n = 10$) and P2RY2 KO ($n = 8$) groups.

(I) Quantification of the lick rates over 15 trials in wild-type and P2RY2 KO mice ($n = 8$ to 10 for each group). Licks in each trial are normalized by the number of licks in the first trial. Solid lines represent the linear regression lines. $p = 0.1165$ in 10 mM, $p = 0.3812$ in 20 mM, $p = 0.0147$ in 30 mM by unpaired t test.

(J) Comparison of adaptation rates in (I) between wild-type and P2RY2 KO mice. The adaptation rate is defined as the absolute value of the slope acquired from simple linear regression. The dotted curves indicate the least-squares fit to the one-phase association. $p = 0.0160$ by unpaired t test.

(K) Re-emergence of sweet adaptation and recovery of maximal licks in the first trial of the subsequent session conducted 2 min after the prior session. Each session consists of 15 consecutive trials of 5-s exposures to 30 mM AceK.

(L and M) Comparison of lick counts and adaptation rate in the first 5-s trial in the first and second sessions. $p = 0.365$ in (L) and $p = 0.9632$ in (M) by unpaired t test.

Please cite this article in press as: Park et al., Glia-like taste cells mediate an intercellular mode of peripheral sweet adaptation, Cell (2025), https://doi.org/10.1016/j.cell.2024.10.041

psychophysics studies suggested that high-potency sweeteners display a higher degree of sweet adaptation in comparison to natural sugars.[86] While we confirmed similar adapting kinetics with fructose (Figure S2N), our experiments are largely constrained to high-potency sweeteners because the high refractive index of most natural sugars introduces severe optical aberrations to the μTongue system.[87] Integration of adaptive optics to the imaging module would resolve this technical limitation. Second, our results show that the inhibitory modulation exerted by type I cells is taste modality-specific (i.e., sweet and bitter); however, the detailed mechanism remains to be investigated. For instance, it is unclear why umami taste rarely elicits calcium responses in type I cells despite sharing the same purinergic neurotransmission mechanism with sweet and bitter taste. The spatial association of specific cellular subtypes may underlie this taste modality-specific influence, which requires further investigation. Third, although intracellular calcium widely serves as a surrogate marker for cellular activity, further studies utilizing electrophysiology or genetically encoded voltage indicators are required to validate our findings at the level of membrane potentials.[88] Lastly, this study is conducted on mouse models, and as such, we cannot preclude the possibility that the same mechanism may not be preserved in other species, including humans. As we identified the clinically applicable agonist for type I cells (i.e., diquafosol), we believe psychophysics studies on human subjects will address this issue in the near future.

RESOURCE AVAILABILITY

Lead contact

Further information and requests for resources and reagents should be directed to and will be fulfilled by the lead contact, Myunghwan Choi, choim@snu.ac.kr.

Materials availability

The LSL-cATP1.0-iP2A-jRGECO1 mouse line, developed by Zhaofa Wu and Yulong Li, is available upon request.

Data and code availability

- The MATLAB code used for analyzing the time-series imaging data is available at the GitHub repository: https://github.com/neurophotonic.
- Any additional information required to reanalyze the data reported in this paper is available from the lead contact upon request.

ACKNOWLEDGMENTS

This work was supported by the Samsung Science and Technology Foundation under project No. SSTF-BA2002-14. We thank Dr. Stephen D. Roper (University of Miami) for providing valuable comments on our manuscript.

AUTHOR CONTRIBUTIONS

J.H. and M.C. initiated this study. M.C. supervised the research. J.H. performed functional screening data on type I cells. G.Y.P. and G.L. performed experiments on the taste bud, analyzed the data, and prepared the figures. M.K. acquired *in situ* hybridization data. S.L. conducted the correlative *in vivo-ex vivo* imaging. J.Y. and C.P. performed experiments on mouse behavior. Z.W. and Y.L. developed a mouse model. G.Y.P., G.L., and M.C. co-wrote the paper. All authors reviewed and edited the paper.

DECLARATION OF INTERESTS

M.C., G.Y.P., and P.C. are inventors of the patent-pending technology regarding the use of diquafosol as a taste-modulatory compound.

STAR★METHODS

Detailed methods are provided in the online version of this paper and include the following:

- KEY RESOURCES TABLE
- EXPERIMENTAL MODEL AND STUDY PARTICIPANT DETAILS
  - Mouse model
- METHOD DETAILS
  - Tastant
  - Pharmacological agonist and antagonist
  - In vivo imaging of the taste bud
  - Cell type identification
  - Image acquisition
  - Multiplex fluorescence in situ hybridization
  - Immunohistochemistry
  - Correlative in vivo – ex vivo imaging
  - Geniculate ganglion surgery
  - Mouse behavior
- QUANTIFICATION AND STATISTICAL ANALYSIS
  - Image analysis
  - Transcriptome analysis of published datasets
  - Statistical Analysis

SUPPLEMENTAL INFORMATION

Supplemental information can be found online at https://doi.org/10.1016/j.cell.2024.10.041.

Received: September 6, 2023
Revised: June 30, 2024
Accepted: October 22, 2024
Published: November 18, 2024

REFERENCES

1. Wark, B., Lundstrom, B.N., and Fairhall, A. (2007). Sensory adaptation. Curr. Opin. Neurobiol. *17*, 423–429. https://doi.org/10.1016/j.conb.2007.07.001.
2. Whitmire, C.J., and Stanley, G.B. (2016). Rapid sensory adaptation redux: a circuit perspective. Neuron *92*, 298–315. https://doi.org/10.1016/j.neuron.2016.09.046.
3. Schwartz, O., and Simoncelli, E.P. (2001). Natural signal statistics and sensory gain control. Nat. Neurosci. *4*, 819–825. https://doi.org/10.1038/90526.
4. Gepshtein, S., Lesmes, L.A., and Albright, T.D. (2013). Sensory adaptation as optimal resource allocation. Proc. Natl. Acad. Sci. USA *110*, 4368–4373. https://doi.org/10.1073/pnas.1204109110.
5. Ferguson, K.A., and Cardin, J.A. (2020). Mechanisms underlying gain modulation in the cortex. Nat. Rev. Neurosci. *21*, 80–92. https://doi.org/10.1038/s41583-019-0253-y.
6. Młynarski, W.F., and Hermundstad, A.M. (2021). Efficient and adaptive sensory codes. Nat. Neurosci. *24*, 998–1009. https://doi.org/10.1038/s41593-021-00846-0.
7. Eagleman, D.M., Jacobson, J.E., and Sejnowski, T.J. (2004). Perceived luminance depends on temporal context. Nature *428*, 854–856. https://doi.org/10.1038/nature02467.
8. Kurahashi, T., and Menini, A. (1997). Mechanism of odorant adaptation in the olfactory receptor cell. Nature *385*, 725–729. https://doi.org/10.1038/385725a0.

Please cite this article in press as: Park et al., Glia-like taste cells mediate an intercellular mode of peripheral sweet adaptation, Cell (2025), https://doi.org/10.1016/j.cell.2024.10.041

9. Merzenich, M.M., and Harrington, T.H. (1969). The sense of flutter-vibration evoked by stimulation of the hairy skin of primates: comparison of human sensory capacity with the responses of mechanoreceptive afferents innervating the hairy skin of monkeys. Exp. Brain Res. *9*, 236–260. https://doi.org/10.1007/BF00234457.

10. Johnson, K.O., and Hsiao, S.S. (1992). Neural mechanisms of tactual form and texture perception. Annu. Rev. Neurosci. *15*, 227–250. https://doi.org/10.1146/annurev.ne.15.030192.001303.

11. Webster, M.A. (2011). Adaptation and visual coding. J. Vis. *11*, 3. https://doi.org/10.1167/11.5.3.

12. Brunton, B.W., Botvinick, M.M., and Brody, C.D. (2013). Rats and humans can optimally accumulate evidence for decision-making. Science *340*, 95–98. https://doi.org/10.1126/science.1233912.

13. Khalighinejad, B., Herrero, J.L., Mehta, A.D., and Mesgarani, N. (2019). Adaptation of the human auditory cortex to changing background noise. Nat. Commun. *10*, 2509. https://doi.org/10.1038/s41467-019-10611-4.

14. Mcburney, D.H. (1972). Gustatory cross adaptation between sweet-tasting compounds. Percept. Psychophys. *11*, 225–227. https://doi.org/10.3758/BF03206254.

15. Kroeze, J.H.A. (1979). Masking and adaptation of sugar sweetness intensity. Physiol. Behav. *22*, 347–351. https://doi.org/10.1016/0031-9384(79)90097-0.

16. Cheung, M., Rivers, N., Breslin, P., and Wise, P. (2021). Individual differences in adaptation to sweet taste. Curr. Dev. Nutr. *5*, 1203. https://doi.org/10.1093/cdn/nzab055_013.

17. Smith, D.V., Bealer, S.L., and Van Buskirk, R.L. (1978). Adaptation and recovery of the rat chorda tympani response to NaCl. Physiol. Behav. *20*, 629–636. https://doi.org/10.1016/0031-9384(78)90256-1.

18. Hellekant, G., Danilova, V., and Ninomiya, Y. (1997). Primate sense of taste: behavioral and single chorda tympani and glossopharyngeal nerve fiber recordings in the rhesus monkey, Macaca mulatta. J. Neurophysiol. *77*, 978–993. https://doi.org/10.1152/jn.1997.77.2.978.

19. Nelson, G., Hoon, M.A., Chandrashekar, J., Zhang, Y., Ryba, N.J.P., and Zuker, C.S. (2001). Mammalian sweet taste receptors. Cell *106*, 381–390. https://doi.org/10.1016/s0092-8674(01)00451-2.

20. Hoon, M.A., Adler, E., Lindemeier, J., Battey, J.F., Ryba, N.J.P., and Zuker, C.S. (1999). Putative mammalian taste receptors: a class of taste-specific GPCRs with distinct topographic selectivity. Cell *96*, 541–551. https://doi.org/10.1016/s0092-8674(00)80658-3.

21. Zhao, G.Q., Zhang, Y., Hoon, M.A., Chandrashekar, J., Erlenbach, I., Ryba, N.J.P., and Zuker, C.S. (2003). The receptors for mammalian sweet and umami taste. Cell *115*, 255–266. https://doi.org/10.1016/s0092-8674(03)00844-4.

22. Ki, S.Y., and Jeong, Y.T. (2022). Taste receptors beyond taste buds. Int. J. Mol. Sci. *23*, 9677. https://doi.org/10.3390/ijms23179677.

23. Max, M., Shanker, Y.G., Huang, L., Rong, M., Liu, Z., Campagne, F., Weinstein, H., Damak, S., and Margolskee, R.F. (2001). Tas1r3, encoding a new candidate taste receptor, is allelic to the sweet responsiveness locus Sac. Nat. Genet. *28*, 58–63. https://doi.org/10.1038/ng0501-58.

24. Schiffman, S.S., Pecore, S.D., Booth, B.J., Losee, M.L., Carr, B.T., Sattely-Miller, E., Graham, B.G., and Warwick, Z.S. (1994). Adaptation of sweeteners in water and in tannic acid solutions. Physiol. Behav. *55*, 547–559. https://doi.org/10.1016/0031-9384(94)90116-3.

25. Zhang, Y., Hoon, M.A., Chandrashekar, J., Mueller, K.L., Cook, B., Wu, D., Zuker, C.S., and Ryba, N.J.P. (2003). Coding of sweet, bitter, and umami tastes: different receptor cells sharing similar signaling pathways. Cell *112*, 293–301. https://doi.org/10.1016/s0092-8674(03)00071-0.

26. Bastiaan-Net, S., van den Berg-Somhorst, D.B.P.M., Ariëns, R.M.C., Paques, M., and Mes, J.J. (2018). A novel functional screening assay to monitor sweet taste receptor activation in vitro. Flavour Fragr. J. *33*, 173–183. https://doi.org/10.1002/ffj.3431.

27. Roper, S.D., and Chaudhari, N. (2017). Taste buds: cells, signals and synapses. Nat. Rev. Neurosci. *18*, 485–497. https://doi.org/10.1038/nrn.2017.68.

28. Liman, E.R., and Kinnamon, S.C. (2021). Sour taste: receptors, cells and circuits. Curr. Opin. Physiol. *20*, 8–15. https://doi.org/10.1016/j.cophys.2020.12.006.

29. Liman, E.R., Zhang, Y.V., and Montell, C. (2014). Peripheral coding of taste. Neuron *81*, 984–1000. https://doi.org/10.1016/j.neuron.2014.02.022.

30. Nomura, K., Nakanishi, M., Ishidate, F., Iwata, K., and Taruno, A. (2020). All-electrical Ca2+-independent signal transduction mediates attractive sodium taste in taste buds. Neuron *106*, 816–829.e6. https://doi.org/10.1016/j.neuron.2020.03.006.

31. Jang, J.H., Kwon, O., Moon, S.J., and Jeong, Y.T. (2021). Recent advances in understanding peripheral taste decoding I: 2010 to 2020. Endocrinol. Metab. (Seoul) *36*, 469–477. https://doi.org/10.3803/EnM.2021.302.

32. Lee, H., MacPherson, L.J., Parada, C.A., Zuker, C.S., and Ryba, N.J.P. (2017). Rewiring the taste system. Nature *548*, 330–333. https://doi.org/10.1038/nature23299.

33. Wilson, C.E., Lasher, R.S., Yang, R., Dzowo, Y., Kinnamon, J.C., and Finger, T.E. (2022). Taste bud connectome: implications for taste information processing. J. Neurosci. *42*, 804–816. https://doi.org/10.1523/JNEUROSCI.0838-21.2021.

34. Kinnamon, S.C., and Finger, T.E. (2019). Recent advances in taste transduction and signaling. F1000Res *8*, F1000FacultyRev-2117. https://doi.org/10.12688/f1000research.21099.1.

35. Dvoryanchikov, G., Sinclair, M.S., Perea-Martinez, I., Wang, T., and Chaudhari, N. (2009). Inward rectifier channel, ROMK, is localized to the apical tips of glial-like cells in mouse taste buds. J. Comp. Neurol. *517*, 1–14. https://doi.org/10.1002/cne.22152.

36. Roper, S.D. (2013). Taste buds as peripheral chemosensory processors. Semin. Cell Dev. Biol. *24*, 71–79. https://doi.org/10.1016/j.semcdb.2012.12.002.

37. Roper, S.D. (2007). Signal transduction and information processing in mammalian taste buds. Pflugers Arch. *454*, 759–776. https://doi.org/10.1007/s00424-007-0247-x.

38. Rodriguez, Y.A., Roebber, J.K., Dvoryanchikov, G., Makhoul, V., Roper, S.D., and Chaudhari, N. (2021). "Tripartite synapses" in taste buds: a role for type I glial-like taste cells. J. Neurosci. *41*, 9860–9871. https://doi.org/10.1523/JNEUROSCI.1444-21.2021.

39. Baumer-Harrison, C., Raymond, M.A., Myers, T.A., Sussman, K.M., Rynberg, S.T., Ugartechea, A.P., Lauterbach, D., Mast, T.G., and Breza, J.M. (2020). Optogenetic stimulation of type I GAD65+ cells in taste buds activates gustatory neurons and drives appetitive licking behavior in sodium-depleted mice. J. Neurosci. *40*, 7795–7810. https://doi.org/10.1523/JNEUROSCI.0597-20.2020.

40. Doyle, M.E., Premathilake, H.U., Yao, Q., Mazucanti, C.H., and Egan, J.M. (2023). Physiology of the tongue with emphasis on taste transduction. Physiol. Rev. *103*, 1193–1246. https://doi.org/10.1152/physrev.00012.2022.

41. Han, J., Choi, P., and Choi, M. (2021). μTongue: a microfluidics-based functional imaging platform for the tongue in vivo. J. Vis. Exp. *170*, e62361. https://doi.org/10.3791/62361.

42. Han, J., and Choi, M. (2018). Comprehensive functional screening of taste sensation in vivo. Preprint at bioRxiv, 371682. https://doi.org/10.1101/371682.

43. Park, G.Y., Hwang, H., and Choi, M. (2022). Advances in optical tools to study taste sensation. Mol. Cells *45*, 877–882. https://doi.org/10.14348/molcells.2022.0116.

44. Wu, Z., Lin, D., and Li, Y. (2022). Pushing the frontiers: tools for monitoring neurotransmitters and neuromodulators. Nat. Rev. Neurosci. *23*, 257–274. https://doi.org/10.1038/s41583-022-00577-6.

Please cite this article in press as: Park et al., Glia-like taste cells mediate an intercellular mode of peripheral sweet adaptation, Cell (2025), https://doi.org/10.1016/j.cell.2024.10.041

45. Taruno, A., Nomura, K., Kusakizako, T., Ma, Z., Nureki, O., and Foskett, J.K. (2021). Taste transduction and channel synapses in taste buds. Pflugers Arch. *473*, 3–13. https://doi.org/10.1007/s00424-020-02464-4.

46. Finger, T.E., Danilova, V., Barrows, J., Bartel, D.L., Vigers, A.J., Stone, L., Hellekant, G., and Kinnamon, S.C. (2005). ATP signaling is crucial for communication from taste buds to gustatory nerves. Science *310*, 1495–1499. https://doi.org/10.1126/science.1118435.

47. Kinnamon, S., and Finger, T. (2022). The role of ATP and purinergic receptors in taste signaling. Handb. Exp. Pharmacol. *275*, 91–107. https://doi.org/10.1007/164_2021_518.

48. Wu, Z., He, K., Chen, Y., Li, H., Pan, S., Li, B., Liu, T., Xi, F., Deng, F., Wang, H., et al. (2022). A sensitive GRAB sensor for detecting extracellular ATP in vitro and in vivo. Neuron *110*, 770–782.e5. https://doi.org/10.1016/j.neuron.2021.11.027.

49. Vandenbeuch, A., Anderson, C.B., Parnes, J., Enjyoji, K., Robson, S.C., Finger, T.E., and Kinnamon, S.C. (2013). Role of the ectonucleotidase NTPDase2 in taste bud function. Proc. Natl. Acad. Sci. USA *110*, 14789–14794. https://doi.org/10.1073/pnas.1309468110.

50. Kinnamon, S.C., and Finger, T.E. (2013). A taste for ATP: neurotransmission in taste buds. Front. Cell. Neurosci. *7*, 264. https://doi.org/10.3389/fncel.2013.00264.

51. Larson, E.D., Vandenbeuch, A., Anderson, C.B., and Kinnamon, S.C. (2021). GAD65Cre drives reporter expression in multiple taste cell types. Chem. Senses *46*, bjab033. https://doi.org/10.1093/chemse/bjab033.

52. Tomchik, S.M., Berg, S., Kim, J.W., Chaudhari, N., and Roper, S.D. (2007). Breadth of tuning and taste coding in mammalian taste buds. J. Neurosci. *27*, 10840–10848. https://doi.org/10.1523/JNEUROSCI.1863-07.2007.

53. Jiang, H., Kuang, Y., Wu, Y., Xie, W., Simon, M.I., and Wu, D. (1997). Roles of phospholipase C β2 in chemoattractant-elicited responses. Proc. Natl. Acad. Sci. USA *94*, 7971–7975. https://doi.org/10.1073/pnas.94.15.7971.

54. Pérez, C.A., Huang, L., Rong, M., Kozak, J.A., Preuss, A.K., Zhang, H., Max, M., and Margolskee, R.F. (2002). A transient receptor potential channel expressed in taste receptor cells. Nat. Neurosci. *5*, 1169–1176. https://doi.org/10.1038/nn952.

55. Communi, D., Parmentier, M., and Boeynaems, J.M. (1996). Cloning, functional expression and tissue distribution of the human P2Y6 receptor. Biochem. Biophys. Res. Commun. *222*, 303–308. https://doi.org/10.1006/bbrc.1996.0739.

56. Waldo, G.L., Corbitt, J., Boyer, J.L., Ravi, G., Kim, H.S., Ji, X.-D., Lacy, J., Jacobson, K.A., and Harden, T.K. (2002). Quantitation of the P2Y1 receptor with a high affinity radiolabeled antagonist. Mol. Pharmacol. *62*, 1249–1257. https://doi.org/10.1124/mol.62.5.1249.

57. Communi, D., Robaye, B., and Boeynaems, J.M. (1999). Pharmacological characterization of the human P2Y11 receptor. Br. J. Pharmacol. *128*, 1199–1206. https://doi.org/10.1038/sj.bjp.0702909.

58. Marteau, F., Le Poul, E., Communi, D., Communi, D., Labouret, C., Savi, P., Boeynaems, J.-M., and Gonzalez, N.S. (2003). Pharmacological characterization of the human P2Y13 receptor. Mol. Pharmacol. *64*, 104–112. https://doi.org/10.1124/mol.64.1.104.

59. Pendergast, W., Yerxa, B.R., Douglass, J.G., Shaver, S.R., Dougherty, R.W., Redick, C.C., Sims, I.F., and Rideout, J.L. (2001). Synthesis and P2Y receptor activity of a series of uridine dinucleoside 5′-polyphosphates. Bioorg. Med. Chem. Lett. *11*, 157–160. https://doi.org/10.1016/s0960-894x(00)00612-0.

60. Lazarowski, E.R., Watt, W.C., Stutts, M.J., Brown, H.A., Boucher, R.C., and Harden, T.K. (1996). Enzymatic synthesis of UTPγS, a potent hydrolysis resistant agonist of P2U-purinoceptors. Br. J. Pharmacol. *117*, 203–209. https://doi.org/10.1111/j.1476-5381.1996.tb15175.x.

61. Lau, O.C.F., Samarawickrama, C., and Skalicky, S.E. (2014). P2Y2 receptor agonists for the treatment of dry eye disease: a review. Clin. Ophthalmol. *8*, 327–334. https://doi.org/10.2147/OPTH.S39699.

62. Liang, Z., Wilson, C.E., Teng, B., Kinnamon, S.C., and Liman, E.R. (2023). The proton channel OTOP1 is a sensor for the taste of ammonium chloride. Nat. Commun. *14*, 6194. https://doi.org/10.1038/s41467-023-41637-4.

63. Rafehi, M., Burbiel, J.C., Attah, I.Y., Abdelrahman, A., and Müller, C.E. (2017). Synthesis, characterization, and in vitro evaluation of the selective P2Y2 receptor antagonist AR-C118925. Purinergic Signal. *13*, 89–103. https://doi.org/10.1007/s11302-016-9542-3.

64. Koh, S. (2015). Clinical utility of 3% diquafosol ophthalmic solution in the treatment of dry eyes. Clin. Ophthalmol. *9*, 865–872. https://doi.org/10.2147/OPTH.S69486.

65. Dvoryanchikov, G., Hernandez, D., Roebber, J.K., Hill, D.L., Roper, S.D., and Chaudhari, N. (2017). Transcriptomes and neurotransmitter profiles of classes of gustatory and somatosensory neurons in the geniculate ganglion. Nat. Commun. *8*, 760. https://doi.org/10.1038/s41467-017-01095-1.

66. Sinclair, M.S., Perea-Martinez, I., Dvoryanchikov, G., Yoshida, M., Nishimori, K., Roper, S.D., and Chaudhari, N. (2010). Oxytocin signaling in mouse taste buds. PLOS One *5*, e11980. https://doi.org/10.1371/journal.pone.0011980.

67. Sinclair, M.S., Perea-Martinez, I., Abouyared, M., St John, S.J., and Chaudhari, N. (2015). Oxytocin decreases sweet taste sensitivity in mice. Physiol. Behav. *141*, 103–110. https://doi.org/10.1016/j.physbeh.2014.12.048.

68. Asencor, A.I., Dvoryanchikov, G., Makhoul, V., Tsoulfas, P., and Chaudhari, N. (2022). Selectively imaging cranial sensory ganglion neurons using AAV-PHP.S. eNeuro *9*, ENEURO.0373-21.2022. https://doi.org/10.1523/ENEURO.0373-21.2022.

69. Bartel, D.L., Sullivan, S.L., Lavoie, E.G., Sévigny, J., and Finger, T.E. (2006). Nucleoside triphosphate diphosphohydrolase-2 is the ecto-ATPase of type I cells in taste buds. J. Comp. Neurol. *497*, 1–12. https://doi.org/10.1002/cne.20954.

70. Lawton, D.M., Furness, D.N., Lindemann, B., and Hackney, C.M. (2000). Localization of the glutamate-aspartate transporter, GLAST, in rat taste buds. Eur. J. Neurosci. *12*, 3163–3171. https://doi.org/10.1046/j.1460-9568.2000.00207.x.

71. Obata, H., Shimada, K., Sakai, N., and Saito, N. (1997). GABAergic neurotransmission in rat taste buds: immunocytochemical study for GABA and GABA transporter subtypes. Brain Res. Mol. Brain Res. *49*, 29–36. https://doi.org/10.1016/s0169-328x(97)00118-6.

72. Cao, Y., Zhao, F.L., Kolli, T., Hivley, R., and Herness, S. (2009). GABA expression in the mammalian taste bud functions as a route of inhibitory cell-to-cell communication. Proc. Natl. Acad. Sci. USA *106*, 4006–4011. https://doi.org/10.1073/pnas.0808672106.

73. Wu, Y., Wang, W., Díez-Sampedro, A., and Richerson, G.B. (2007). Nonvesicular inhibitory neurotransmission via reversal of the GABA transporter GAT-1. Neuron *56*, 851–865. https://doi.org/10.1016/j.neuron.2007.10.021.

74. Lee, S., Yoon, B.-E., Berglund, K., Oh, S.-J., Park, H., Shin, H.-S., Augustine, G.J., and Lee, C.J. (2010). Channel-mediated tonic GABA release from glia. Science *330*, 790–796. https://doi.org/10.1126/science.1184334.

75. Huang, Y.J., Maruyama, Y., Lu, K.S., Pereira, E., Plonsky, I., Baur, J.E., Wu, D., and Roper, S.D. (2005). Mouse taste buds use serotonin as a neurotransmitter. J. Neurosci. *25*, 843–847. https://doi.org/10.1523/JNEUROSCI.4446-04.2005.

76. Huang, Y.A., Dando, R., and Roper, S.D. (2009). Autocrine and paracrine roles for ATP and serotonin in mouse taste buds. J. Neurosci. *29*, 13909–13918. https://doi.org/10.1523/JNEUROSCI.2351-09.2009.

77. Ralevic, V., and Burnstock, G. (1998). Receptors for Purines and Pyrimidines. Pharmacol. Rev. *50*, 413–492.

78. Glaser, T., Resende, R.R., and Ulrich, H. (2013). Implications of purinergic receptor-mediated intracellular calcium transients in neural differentiation. Cell Commun. Signal. *11*, 12. https://doi.org/10.1186/1478-811X-11-12.

Please cite this article in press as: Park et al., Glia-like taste cells mediate an intercellular mode of peripheral sweet adaptation, Cell (2025), https://doi.org/10.1016/j.cell.2024.10.041

79. Schmitt, R.O., Dev, P., and Smith, B.H. (1976). Electrotonic processing of information by brain cells. Science *193*, 114–120. https://doi.org/10.1126/science.180598.

80. Shepherd, G.M. (2003). The Synaptic Organization of the Brain (Oxford University Press).

81. Barlow, H.B. (1961). Possible principles underlying the transformation of sensory messages. Sens. Commun. *1*, 217–233.

82. Anstis, S., and Saida, S. (1985). Adaptation to auditory streaming of frequency-modulated tones. J. Exp. Psychol. Hum. Percept. Perform. *11*, 257–271. https://doi.org/10.1037/0096-1523.11.3.257.

83. Martinez-Conde, S., Macknik, S.L., and Hubel, D.H. (2004). The role of fixational eye movements in visual perception. Nat. Rev. Neurosci. *5*, 229–240. https://doi.org/10.1038/nrn1348.

84. Fairhall, A.L., Lewen, G.D., Bialek, W., and De Ruyter Van Steveninck, R.R. (2001). Efficiency and ambiguity in an adaptive neural code. Nature *412*, 787–792. https://doi.org/10.1038/35090500.

85. Blednov, Y.A., Walker, D.L., Iyer, S.V., Homanics, G., and Harris, A.R. (2010). Mice lacking Gad2 show altered behavioral effects of ethanol, flurazepam and gabaxadol. Addict. Biol. *15*, 45–61. https://doi.org/10.1111/j.1369-1600.2009.00186.x.

86. Bornstein, B.L., Wiet, S.G., and Pombo, M. (1993). Sweetness adaptation of some carbohydrate and high potency sweeteners. J. Food Sci. *58*, 595–598. https://doi.org/10.1111/j.1365-2621.1993.tb04332.x.

87. Han, J., Kim, S., Choi, P., Lee, S., Jo, Y., Kim, E., and Choi, M. (2021). Robust functional imaging of taste sensation with a Bessel beam. Biomed. Opt. Express *12*, 5855–5864. https://doi.org/10.1364/BOE.430643.

88. Knöpfel, T., and Song, C. (2019). Optical voltage imaging in neurons: moving from technology development to practical tool. Nat. Rev. Neurosci. *20*, 719–727. https://doi.org/10.1038/s41583-019-0231-4.

89. Kim, A.Y., Tang, Z., Liu, Q., Patel, K.N., Maag, D., Geng, Y., and Dong, X. (2008). Pirt, a Phosphoinositide-Binding Protein, Functions as a Regulatory Subunit of TRPV1. Cell *133*, 475–485. https://doi.org/10.1016/j.cell.2008.02.053.

90. Lionnet, T., Czaplinski, K., Darzacq, X., Shav-Tal, Y., Wells, A.L., Chao, J.A., Park, H.Y., De Turris, V., Lopez-Jones, M., and Singer, R.H. (2011). A transgenic mouse for in vivo detection of endogenous labeled mRNA. Nat. Methods *8*, 165–170. https://doi.org/10.1038/nmeth.1551.

91. Fowler, B.E., Ye, J., Humayun, S., Lee, H., and Macpherson, L.J. (2022). Regional specialization of the tongue revealed by gustatory ganglion imaging. iScience *25*, 105700. https://doi.org/10.1016/j.isci.2022.105700.

92. Imbert, A., Ouyang, W., Safieddine, A., Coleno, E., Zimmer, C., Bertrand, E., Walter, T., and Mueller, F. (2022). FISH-quant v2: a scalable and modular tool for smFISH image analysis. RNA *28*, 786–795. https://doi.org/10.1261/rna.079073.121.

93. Berger, D.R., Seung, H.S., and Lichtman, J.W. (2018). VAST (Volume Annotation and Segmentation Tool): Efficient manual and semi-automatic labeling of large 3D image stacks. Front. Neural Circuits *12*, 88. https://doi.org/10.3389/fncir.2018.00088.

94. Bishop, D., Nikić, I., Brinkoetter, M., Knecht, S., Potz, S., Kerschensteiner, M., and Misgeld, T. (2011). Near-infrared branding efficiently correlates light and electron microscopy. Nat. Methods *8*, 568–570. https://doi.org/10.1038/nmeth.1622.

95. Fowler, B.E., and Macpherson, L.J. (2021). In vivo calcium imaging of mouse geniculate ganglion neuron responses to taste stimuli. J. Vis. Exp. *168*, 1–11. https://doi.org/10.3791/62172.

96. Pnevmatikakis, E.A., and Giovannucci, A. (2017). NoRMCorre: An online algorithm for piecewise rigid motion correction of calcium imaging data. J. Neurosci. Methods *291*, 83–94. https://doi.org/10.1016/j.jneumeth.2017.07.031.

97. Guizar-Sicairos, M., Thurman, S.T., and Fienup, J.R. (2008). Efficient subpixel image registration algorithms. Opt. Lett. *33*, 156–158. https://doi.org/10.1364/ol.33.000156.

98. Zhou, P., Resendez, S.L., Rodriguez-Romaguera, J., Jimenez, J.C., Neufeld, S.Q., Giovannucci, A., Friedrich, J., Pnevmatikakis, E.A., Stuber, G.D., Hen, R., et al. (2018). Efficient and accurate extraction of in vivo calcium signals from microendoscopic video data. eLife *7*, e28728. https://doi.org/10.7554/eLife.28728.

99. Pnevmatikakis, E.A., Soudry, D., Gao, Y., Machado, T.A., Merel, J., Pfau, D., Reardon, T., Mu, Y., Lacefield, C., Yang, W., et al. (2016). Simultaneous denoising, deconvolution, and demixing of calcium imaging data. Neuron *89*, 285–299. https://doi.org/10.1016/j.neuron.2015.11.037.

Please cite this article in press as: Park et al., Glia-like taste cells mediate an intercellular mode of peripheral sweet adaptation, Cell (2025), https://doi.org/10.1016/j.cell.2024.10.041

STAR★METHODS

KEY RESOURCES TABLE

REAGENT or RESOURCE	SOURCE	IDENTIFIER
Chemicals, peptides, and recombinant proteins		
Sodium chloride	Sigma-Aldrich	Cat#S9888
Potassium chloride	Sigma-Aldrich	Cat#P3911
Sodium bicarbonate	Sigma-Aldrich	Cat#S6014
Potassium bicarbonate	Sigma-Aldrich	Cat#237205
Calcium chloride solution	Sigma-Aldrich	Cat#21115
Magnesium chloride	Sigma-Aldrich	Cat#M8266
Potassium phosphate dibasic	Sigma-Aldrich	Cat#P3786
Potassium phosphate monobasic	Sigma-Aldrich	Cat#P0662
Hydrochloric acid	Sigma-Aldrich	Cat#320331
Suramin sodium salt	Sigma-Aldrich	Cat#S2671
Adenosine 5‘-triphosphate disodium salt hydrate	Sigma-Aldrich	Cat#A2383
Adenosine 5‘-diphosphate disodium salt	Sigma-Aldrich	Cat#01897
Uridine 5‘-triphosphate trisodium salt hydrate	Sigma-Aldrich	Cat#U6750
Uridine 5‘-diphosphate disodium salt hydrate	Sigma-Aldrich	Cat#94330
2′(3′)-O-(4-Benzoylbenzoyl)adenosine 5′-triphosphate triethylammonium salt (Benzoylbenzoyl-ATP)	Sigma-Aldrich	Cat#B6396
Adenosine 5′-[γ-thio]triphosphate tetralithium salt (ATP-γ-s)	Sigma-Aldrich	Cat#A1388
Uridine 5‘-O-(3-thiotriphosphate) (UTP-γ-s)	Biolog	Cat#U010-05
Oxytocin	Sigma-Aldrich	Cat#O3251
Diquafosol sodium	Santen pharmaceutical	Diquas-S
AR-C 118925	Tocris Bioscience	Cat#4890/5
Acesulfame K	Sigma-Aldrich	Cat#04054
Sucralose	Sigma-Aldrich	Cat#69293
Sodium saccharin	Sigma-Aldrich	Cat#47839
Citric acid	Sigma-Aldrich	Cat#C0759
L-glutamic acid monopotassium salt monohydrate	Sigma-Aldrich	Cat#49601
Inosine 5‘-monophosphate disodium salt hydrate	Sigma-Aldrich	Cat#I4625
Quinine hydrochloride dihydrate	Sigma-Aldrich	Cat#Q1125
Denatonium benzoate	Sigma-Aldrich	Cat#D5765
Cycloheximide	Sigma-Aldrich	Cat#01810
Tetramethylrhodamine isothiocyanate-Dextran (500 kDa)	Sigma-Aldrich	Cat#52194
Experimental models: Organisms/strains		
Mouse: *Pirt-Cre*	Kim et al.[89]	N/A
Mouse: *GAD65-Cre*	Jackson Laboratory	Cat#010802
Mouse: B6(129S4)-*Gt(ROSA) 26Sor*$^{tm1.1(CAG-tdTomato/GCaMP6f)Mdcah}$/J	Jackson Laboratory	Cat#031968

(*Continued on next page*)

Please cite this article in press as: Park et al., Glia-like taste cells mediate an intercellular mode of peripheral sweet adaptation, Cell (2025), https://doi.org/10.1016/j.cell.2024.10.041

Continued

REAGENT or RESOURCE	SOURCE	IDENTIFIER
Mouse: LSL-cATP1.0-iP2A-jRGECO1	This paper	N/A
Mouse: B6(129S6)-*Polr2a*$^{Tn(pb\text{-}CAG\text{-}tdTomato/GCaMP5g)Tvrd}$/J	Jackson Laboratory	Cat#024477
Mouse: B6(129S1)-*Plcb2*^{tm1Dwu}/J	Jackson Laboratory	Cat#018064
Mouse: B6(129P2)-*P2ry2*^{tm1Bhk}/J	Jackson Laboratory	Cat#009132
rAAV: AAV::PHP.S-CAG-GCaMP6f-WPRE-SV40	This paper	N/A
Software and algorithms		
Fiji – ImageJ 2.3.0	NIH	RRID:SCR_002285; URL: http://fiji.sc
NIS-Elements	Nikon	RRID:SCR_014329; URL: https://www.nikoninstruments.com/Products/Software
MATLAB 2021b	Mathworks	RRID:SCR_001622; URL: http://www.mathworks.com/products/matlab/
CaImAn-MATLAB	Flatiron Institute	URL: https://github.com/flatironinstitute/CaImAn-MATLAB
Airlocalize - MATLAB	Timothee Lionnet et al.[90]	URL: https://github.com/timotheelionnet/AIRLOCALIZE
Adobe Photoshop	Adobe	RRID:SCR_014199; URL: https://www.adobe.com/products/photoshop.html
GraphPad Prism 9	GraphPad	RRID:SCR_002798; URL: http://www.graphpad.com/
R project for statistical computing	R project	RRID:SCR_001905; URL: http://www.r-project.org/

EXPERIMENTAL MODEL AND STUDY PARTICIPANT DETAILS

Mouse model

All mice were housed in groups of two to five per cage under a reversed 12:12-hour light/dark cycle where temperature (22–23°C) and humidity (40–60%) were maintained. They were given ad libitum access to food and water. Both sexes of mice older than at least 7 weeks were used in experiments. There was no significant difference between male and female mice. All animal experiments were performed in compliance with institutional guidelines and approved by the subcommittee for research animal care at Seoul National University.

For the studies involving wild-type mice, 8- to 12-week-old C57BL/6 mice (Orient Bio and Saeron Bio) were used. For the studies involving type II/III cells and gustatory afferent nerves labeled by a genetically-encoded calcium indicator, Pirt-GCaMP6f-tdTomato mice were bred by crossing Pirt–Cre mice (provided by Xinzhong Dong at Johns Hopkins University) and CAG-floxed-GCaMP6f-tdTomato mice (#031968, Jackson Laboratory). For the studies involving type I cells expressing genetically encoded calcium indicators, GAD65-GCaMP6f-tdTomato mice were bred by crossing GAD65-Cre mice (#010802, Jackson Laboratory) and CAG-floxed-GCaMP6f-tdTomato mice (#031968, Jackson Laboratory). For the studies measuring intragemmal ATP level, either Pirt-Cre mice or GAD65-Cre mice were crossed with LSL-cATP1.0-iP2A-jRGECO1 mice (created by the Yulong Li Lab at Peking University), producing Pirt-cATP1.0-iP2A-jRGECO1 mice and GAD65-cATP1.0-iP2A-jRGECO1 mice. These reporter mice were also used in experiments at the age of 7-20 weeks. For the studies investigating calcium activities from the gustatory afferent nerve, mice with the desired genetic background (e.g., P2RY2 knockout mice) were infected with AAV.PHP.S-CAG-GCaMP6f-WPRE-SV40 virus via the intravenous route. The virus was assembled using plasmids encoding the viral capsids of AAV.PHP.S serotype (pUCmini-iCAP-PHP.S; #103006, Addgene) and the cargo (pAAV-CAG-GCaMP6f-WPRE-SV40; #100836, Addgene) and it was concentrated to a titer of $\sim 3.6\times10^{13}$ genome copies/mL (IBS Virus Facility). In 4–6-week-old mice the virus was administered through intravenous injection via a retro-orbital route (50 μl corresponding to $\sim 1.8\times10^{12}$ viral genome copies) using a 31G insulin syringe. The mice were then used for afferent taste nerve imaging approximately 3 weeks after the injection.

For the studies investigating type I cells in mice lack of sweet reception, Plcb2 KO mice (#018064, Jackson Laboratory) were crossed with CAG-floxed-GCaMP5g-tdTomato mice (#024477, Jackson Laboratory) resulting in a heterogeneous F1. By F1 cross-breeding, homogeneous CAG-floxed-GcaMP5g-tdTomato-Plcb2KO mice were born. The same procedure was done on Plcb2 KO mice and GAD65-Cre mice, giving birth to GAD65-Cre-Plcb2KO mice. In turn, GAD65-GCaMP5g-tdTomato-Plcb2KO were bred by crossing CAG-floxed-GCaMP5g-tdTomato-Plcb2KO mice and GAD65-Cre-Plcb2KO mice. Similarly, P2RY2 KO GAD2-GCaMP6f-tdTomato mice were generated by crossing P2RY2 KO mice (#009132, Jackson Laboratory) with CAG-floxed-GCaMP6f-tdTomato mice (#031968, Jackson Laboratory).

Please cite this article in press as: Park et al., Glia-like taste cells mediate an intercellular mode of peripheral sweet adaptation, Cell (2025), https://doi.org/10.1016/j.cell.2024.10.041

METHOD DETAILS

Tastant

Artificial saliva was prepared by mixing 2 mM NaCl, 5 mM KCl, 3 mM $NaHCO_3$, 3 mM $KHCO_3$, 0.25 mM $CaCl_2$, 0.25 mM $MgCl_2$, 0.12 mM K_2HPO_4, 0.12 mM KH_2PO_4, and 1.8 mM HCl, and pH was adjusted to 7.4–7.6 by adding 0.1N HCl. Tastant solutions were prepared by adding solute to the artificial saliva (sweet: 10–80 mM AceK, 22.6 mM sodium saccharin, and 20 mM sucralose; bitter: a mixture of 5 mM quinine, 5 mM denatonium, and 0.05 mM cycloheximide; salty: 150 mM NaCl. sour, 10 mM citric acid; umami: 150 mM MPG and 1 mM IMP).[91]

Pharmacological agonist and antagonist

Agonists and antagonists were prepared by adding solutes to phosphate-buffered saline (PBS) for intravenous and submucosal injection or artificial saliva for oral delivery on the tongue. Topically delivered purinergic agonists to the tongue include 1 mM ATP, 1 mM ADP, 1 mM UTP, 1 mM UDP, 1 mM BzATP, 150 μM ATPγS, 150 μM UTPγs, 1 mM 2-MeSATP, and 1 mM diquafosol. Intravenously delivered agonists include 5 mM ATP, 5 mM ATPγS, 5 mM UTP, and 38 mM diquafosol with an injection volume of 100 μl each. Intraperitoneal delivery was used for oxytocin (0.1 mg/kg). Submucosal injection was used for P2RY2 antagonist AR-C (10 μM, 4 μl).

In vivo imaging of the taste bud

The μTongue system was used for the controlled delivery of tastants of interest to the dorsal surface of the tongue.[41,42] In brief, μTongue was assembled by gluing the top and bottom pieces together with a thermoplastic resin to form a microfluidic channel, where tastants can be infused. The 8-channel fluidic delivery system (Octaflow II, ALA Scientific) was connected to the input port of the microfluidic channel via an 8-port manifold (MPP-8, Harvard Apparatus). The outlet of the microfluidic channel was connected to a syringe pump to maintain the flow rate at ∼300 μl/min. The reliability of tastant delivery on the fungiform taste bud was confirmed intermittently by perfusing a fluorescent solution.

For imaging, the mouse was anesthetized by intraperitoneal injection of ketamine (100 mg/kg) along with either xylazine (10 mg/kg) or dexmedetomidine (1 mg/kg). The depth of anesthesia was monitored intermittently using a toe pinch reflex. After removing the scalp and periosteum, a custom head fixer was affixed to the cranium with super glue and dental resin. The mouse head was affixed using the head fixer in a supine position, and then the tongue was withdrawn carefully by a set of cotton tips. The ventral side of the tongue was affixed on a metal fixative using a tissue adhesive. During the preparation, the dorsal surface of the tongue was immersed with artificial saliva to prevent dehydration. After setting up the μTongue system, a twisted tissue paper was placed at the posterior side of the tongue to prevent the risk of suffocation by the leaked solution. TRITC-dextran (3% w/v in saline, 500 kDa; #52194, Sigma-Aldrich) was intravenously injected through the retro-orbital sinus to confirm the intact blood perfusion as well as to easily locate the taste buds.

Cell type identification

Cell types were discerned based on the spatial segregation of calcium responses along the axial axis of the taste bud. Calcium activity in sweet-sensing type II cells manifested predominantly at the apical tip, while afferent nerve calcium responses were confined to the depths of >12 μm from the apical tip (Figures S1G and S1H). Additionally, distinct from type II cells, type I cell responses demonstrated whole-cell cytoplasmic responses across the apical to basal plane. This spatial distinction allowed for unambiguous identification of type I cell responses in the basolateral planes, even with non-specific labeling of type II cells in GAD2-GCaMP-tdTomato mice. For additional verification of the cell type, oxytocin (0.1 mg/kg) was administered intraperitoneally to selectively activate type I cells (Figures S4I and S4J).

Image acquisition

For functional imaging of intracellular calcium and extracellular ATP dynamics, time-series images were acquired by an upright spinning disk confocal microscope, unless otherwise indicated. The spinning disk unit (CSU-W1, Yokogawa; CMCI at Seoul National University) equips with a dual sCMOS camera (Prime BSI, Teledyne Photometrics) for simultaneous acquisition of GCaMP (green) and tdTomato (red) channels. The spinning disk unit is coupled to a multi-line fiber-coupled laser comprising 405, 488, 561, and 640 nm lasers (iChrome MLE, Toptica Photonics), and is connected to the motorized upright microscope body (Ni-U, Nikon). The maximum laser power at the objective back aperture was measured to be 5–10 mW each. The objective z-piezo stage with a 40X water-immersion objective lens (MRD07420, Nikon; NA = 0.8, working distance = 3.5 mm) was used for multi-slice acquisition of individual taste buds (typically, 3-4 slices per taste bud at a volume rate of ∼5 Hz). The image acquisition was controlled by the NIS-Elements software. Some data was acquired by a two-photon microscope (Bergamo II, Thorlabs) coupled to a 920 nm femtosecond fiber laser (FemtoFiber Ultra 920, Toptica Photonics). The laser was scanned via a pair of galvanometric mirrors, and emission was captured by GaAsP photomultipliers. The laser power at the objective back aperture was set to <25 mW to avoid phototoxicity. The image was acquired at a frame rate of ∼5 Hz at a fixed axial position, which was controlled by the ThorImageLS software.

Please cite this article in press as: Park et al., Glia-like taste cells mediate an intercellular mode of peripheral sweet adaptation, Cell (2025), https://doi.org/10.1016/j.cell.2024.10.041

Multiplex fluorescence in situ hybridization

The anterior portion of the mouse tongue was excised under deep anesthesia with ketamine and xylazine. The tongue and geniculate ganglion were frozen in a frozen section media (FSC 22, Leica), and sliced by a cryostat (#CM1860, Leica) at a thickness of 10 μm. The sections were mounted on a pre-coated glass slide (22-037-246, Fisher Scientific), dehydrated at -20°C for 1 h, and stored at -80°C freezer for up to 3 months. For mRNA labeling, a multiplexed RNAscope assay with P2RY2, P2RY4, TAS1R2, TAS1R3, CAR4, GAD2, and ENTPdase2 probes was performed according to the vendor's protocol (RNAscope HiPlex, ADCBio). The mounted sections of the tongue were fixed by immersion in a 10% neutral buffered formalin solution (HT5012, Sigma Aldrich) for 1 h at room temperature and then washed three times with phosphate-buffered saline (10010, Thermo Fisher Scientific). The sections were dehydrated and permeabilized through sequential immersion with 50%, 70%, and 100% ethanol. After drying the sections for 5 minutes, protease III was applied for ~20 minutes to further increase permeabilization. Subsequently, the mRNAs were labeled by hybridization with the probes and the hybridized signals were amplified. Following amplification, up to three types of target fluorophores (Alexa fluor 488, Dylight 550, Dylight 650) and DAPI were applied for each round to label the target mRNAs and nuclei, respectively. Fluorescence images of the samples were acquired using a spinning-disk confocal microscope (CSU-W1, Nikon). For the next round, the tail regions of the probe and the mounting media were removed and then a new set of fluorescent probes was applied to label other hybridized mRNAs. Images from different rounds were registered with DAPI images by using the HiPlex Image Registration Software v2.0.1. For quantification of the mRNA signals, Big-Fish-Quant v2 software was used to extract the spatial distribution of the mRNA signals.[92] The number of mRNA transcripts was counted for each DAPI-labeled nucleus using the VAST software.[93]

Immunohistochemistry

After deep anesthesia, the mouse was transcardially perfused with 4°C saline, followed by 4% paraformaldehyde. The extracted tongue was immersed in the 4% paraformaldehyde at 4°C for 12 hours and subsequently in 30% sucrose solution for 3 days for dehydration. The dehydrated tongue was frozen in a frozen-section media (FSC 22, Leica) and sliced by a cryostat (#CM1860, Leica) at a thickness of 10 to 40 μm. The primary antibodies used were goat anti–mCA4 (1:250; AF2414, R&D Systems), guinea pig anti–mTRPM5 (1:1000; Taste Research Center, Yonsei University), rabbit anti–mNTPDase2 (1:250; ectonucleotidases-ab.com),[69] and rabbit anti-P2RY2 (1:250; APR-010; Alomone Labs). Secondary antibodies used were Alexa Fluor 647 donkey anti–rabbit IgG (A-31573, Thermo Fisher Scientific), Alexa Fluor 633 donkey anti–goat IgG (A-21082, Thermo Fisher Scientific), Alexa Fluor 647 goat anti–guinea pig (ab150187, Abcam), and Alexa Fluor 488 goat anti-rabbit (ab150077, Abcam).

Correlative in vivo – ex vivo imaging

After functional imaging on μTongue, the anesthetized mouse was perfused transcardially with 4% paraformaldehyde. The excised tongue was mounted under a multi-photon microscope for near-infrared branding (NIRB) near the taste bud imaged in vivo.[94] The tongue was sliced en face using a vibratome at a thickness of ~140 μm, incubated in 70% ethanol at room temperature for an hour, and labeled with a TAS1R2 FISH probe. In vivo imaging data was aligned with ex vivo FISH data by applying a rigid registration algorithm in ImageJ.

Geniculate ganglion surgery

For imaging geniculate neurons, the geniculate ganglion was surgically accessed following the previous report by Fowler et al.[95] Briefly, a PIRT-GCaMP-tdTomato mouse was anesthetized with ketamine and xylazine (100 mg/kg and10 mg/kg, respectively) and mounted in a supine position with the cranium affixed to a custom-built head fixer. A tracheotomy was conducted to maintain physiological respiration. Fine forceps were used to expose the geniculate ganglion by opening the tympanic bulla. Tastant solutions were administered to the externalized tongue at a constant flow rate of ~300 μl/min via the Octaflow system, while geniculate neurons were concurrently imaged using a widefield fluorescence microscope with a long working distance objective lens (Nikon, 10X, 0.3 NA).

Mouse behavior

The behavior studies were conducted using the Davis Rig lickometer (MED-DAV-160M, Med Associates), which provides sequential access to 16 different sipper bottles to a mouse in a programmable manner (Figures 6A and 6B). The positioning of the sipper bottles and the opening of the shutter were fully motorized and were controlled by the software (SOF-770, Med Associates). While the sipper bottle was moving into a position, the shutter remained closed preventing the mouse from interacting with the bottle prematurely. When the target bottle was in place, the shutter opened, permitting the mouse to lick the bottle for a duration of 5 s. The capacitive touch sensor (i.e., lickometer) recorded each lick event over time in millisecond precision. Each mouse was trained for 2 days ('training session') prior to the 'testing session'. A total of 10 wildtype mice of both sexes (8 male and 2 female) were used for the study with diquafosol (Figures 6C and 6D), and an additional 7 P2RY2 knockout mice of both sexes (5 male and 2 female) were included for the study on P2RY2 (Figures 6E and 6F). All mice went through the same training and testing sessions for days 1–7, and the testing sessions on days 8–10 were additionally performed for the study with diquafosol.

For day 1 of the training session, a mouse deprived of water for 24 hours prior to the session was given access to the sipper bottle containing water for 20 minutes to get familiarized with the experimental context in the Davis Rig. After completion of each session, the mouse was given *ad libitum* water access for 30 minutes before returning to the water-deprived home cage. On day 2, the mouse

Please cite this article in press as: Park et al., Glia-like taste cells mediate an intercellular mode of peripheral sweet adaptation, Cell (2025), https://doi.org/10.1016/j.cell.2024.10.041

was allowed sequential brief access to six sipper bottles all containing water in a randomized sequence (5 trials per bottle, a total of 30 trials). Each trial consisted of opening the shutter, waiting for the first lick for up to 20 s, 5 s of access to a water bottle, and closing the shutter for 10 s (15–35 s per trial, depending on the timing of the first lick). If the mouse did not lick for the waiting period of 20 s, the trial is closed and moved on to the next trial. Typically, each training session involving 30 trials was completed in 30 min. This protocol maintained the mice's body weights at ~90% of the controls.

For the next 5 days of the testing sessions (days 3–7), all trained mice (n = 17 mice; 10 wild-type and 7 knockout mice) were randomly given four sipper bottles each containing 0 mM, 10 mM, 20 mM, or 30 mM AceK. Each trial was conducted with the same protocol as the training session: opening the shutter, waiting for the first lick for up to 20 s, 5 s of access to a bottle, and closing the shutter for 10 s. To minimize the impact of the sequence, six randomly selected permutations for the 4 bottles were presented for each session (6 × 4 = 24 trials per session) ensuring that no bottles were presented twice in a row. In addition, one trial was followed to cover all possible neighboring binary sequences twice (i.e., a total of 25 trials).

For the diquafosol study (Figures 6A–6F; n = 10 mice), the additional testing sessions on days 8–10 proceeded. The mouse was pre-exposed to either diquafosol (38 mM in saline) or saline control during the initial three or more trials until the lick count exceeds 50. Subsequently, with the same protocol as the prior testing sessions, the mouse was randomly given four sipper bottles each containing 0 mM, 10 mM, 20 mM, or 30 mM AceK for 25 trials (Figures 6A and 6B). The diquafosol and control sessions were repeated in turn on days 8–10.

The sweet adaptation study (Figures 6G–6M) consisted of two parts: the preconditioning session and the main test session. During the preconditioning session, mice were exposed to a randomized sequence of solutions containing 0, 10, 20, and 30 mM AceK. This session continued until the mouse exhibited a reduced number of licks to water, defined as fewer than 10 licks per 5-s access period. This criterion ensured that mice were not excessively thirsty and demonstrated a preference for AceK solutions over water, establishing a baseline for assessing sweet taste adaptation, wherein a decrease in the number of licks would indicate a perceived reduction in sweetness. Once the mouse demonstrated a discernible preference for the sweetened solutions over water, it proceeded to the main test session. In the main test session, each mouse underwent 15 trials with repeated access to a single concentration of AceK (10, 20, or 30 mM). The number of licks for each 5-s trial was quantified.

QUANTIFICATION AND STATISTICAL ANALYSIS

Image analysis

The image analysis pipeline was implemented based on Matlab- or Python-based open-source algorithms developed for calcium imaging data (CaImAn).[96,97] First, the motion artifact was corrected with a non-rigid motion correction algorithm, NoRMCorre. Next, the calcium traces with corresponding ROIs were extracted using the constrained nonnegative matrix factorization algorithm, CNMF-E, which effectively decomposed cellular ROIs based on spatiotemporal calcium dynamics.[98,99] The calcium traces were converted to ΔF/F (i.e., the change in fluorescence divided by the baseline fluorescence). For visualization, image brightness and contrast were linearly adjusted in ImageJ (NIH) or Photoshop (Adobe).

Transcriptome analysis of published datasets

Single-cell FASTQ files for the geniculate ganglion deposited by Dvoryanchikov et al. were obtained from NCBI Gene Expression Omnibus (GSE102443).[65] Raw reads were processed by filtering, scaling, mapping, and quantification. Hierarchical clustering analysis, scaled to each geniculate neuron, was used for further characterization.

Statistical Analysis

The Prism 9 software (GraphPad) and R (R Foundation for Statistical Computing) were used for statistical analysis. Parameters for statistical analyses such as the response delay (Δt), peak ΔF/F, area under curve (AUC), or 1/e duration ($t_{1/e}$) were acquired by Matlab (Mathworks). The heatmaps presenting processed trace data were created with R. The data in heatmaps were either sorted by a parameter (e.g., Δt for Figure 1K) or by the hierarchical clustering analysis using the Ward's method ('Ward.D2' in R; e.g., Figure 1H). For statistical comparison of a parameter between two groups, either paired (Wilcoxon matched-pairs signed rank) or unpaired (Mann-Whitney) t test were used as indicated. For statistical comparison of a parameter among more than two groups, one-way ANOVA was used. The Kolmogorov-Smirnov test was used for statistical comparison between cumulative distribution functions. All the tests were two-sided and the p-values lower than 0.05 were considered statistically significant.

CellPress

Supplemental figures

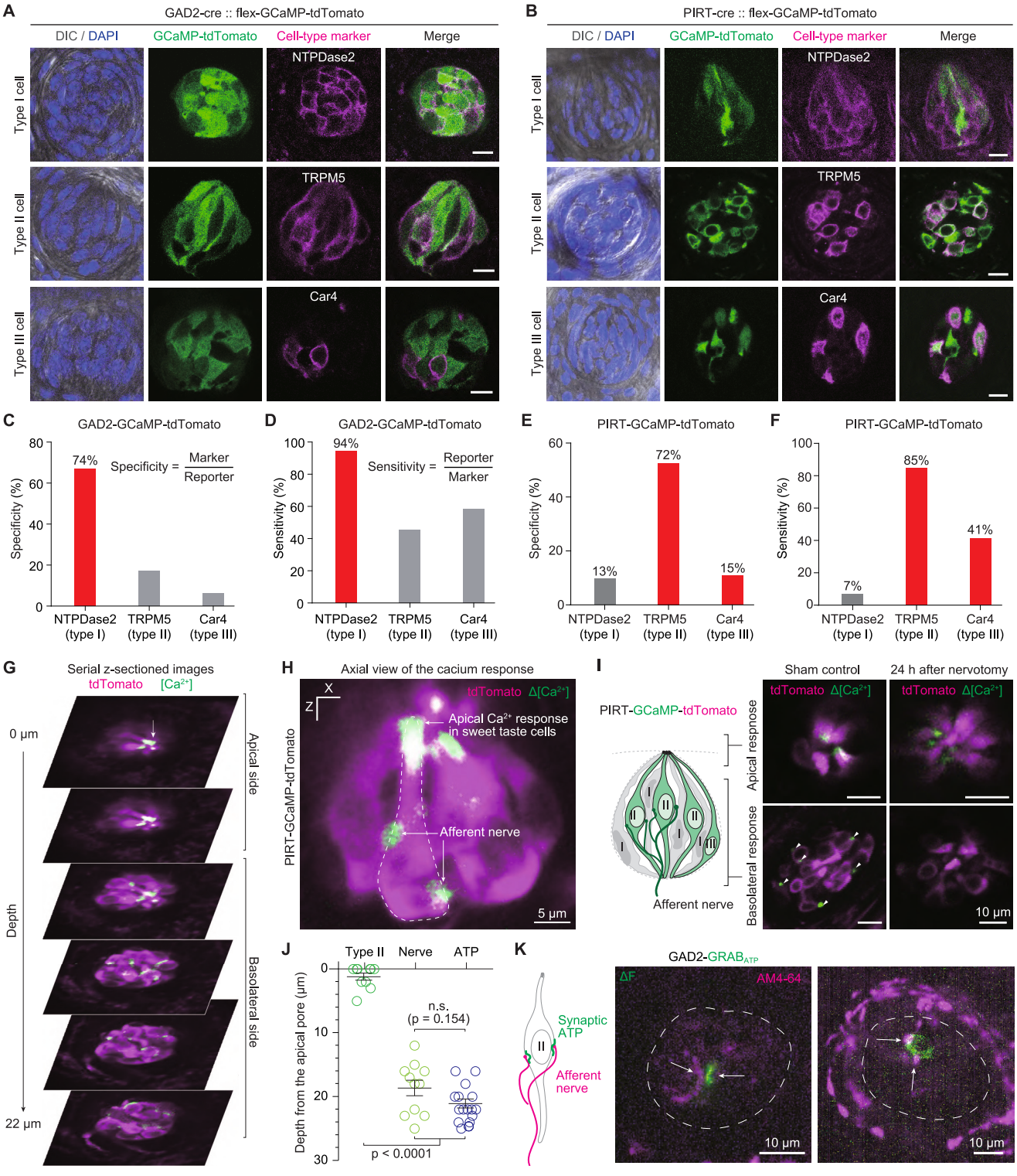

(legend on next page)

Figure S1. Characterization of mouse models, related to Figure 1

(A and B) Representative fluorescence images of GAD2 and PIRT reporter mice showing NTPDase2 (type I cell marker), TRPM5 (type II cell marker), and Car4 (type III cell marker). Scale bar, 10 μm. (n = 2 mice).

(C–F) Specificity and sensitivity of the reporter mice.

(G and H) Axial profile of the sweet-evoked calcium responses in the taste bud (30 mM AceK) of a PIRT-GCaMP-tdTomato mouse (magenta: tdTomato, green: calcium response in ΔF).

(I) Validation of the nerve response on the basolateral side. The puncta-like calcium responses in the basolateral region completely disappeared 24 h after surgical transection of the chorda tympani nerve. Scale bar, 10 μm.

(J) Depth profile of functional responses to 30 mM AceK. Afferent nerve response and synaptic ATP release occurred at depths of ~20 μm, in contrast with the type II cell responses localized to the apical tip.

(K) Spatial correspondence of ATP and afferent nerve responses. The afferent nerve is labeled by intraperitoneal injection of FM4-64 (0.2 mg/mL) to a GAD2-$GRAB_{ATP}$ mouse, 24 h prior to the imaging.

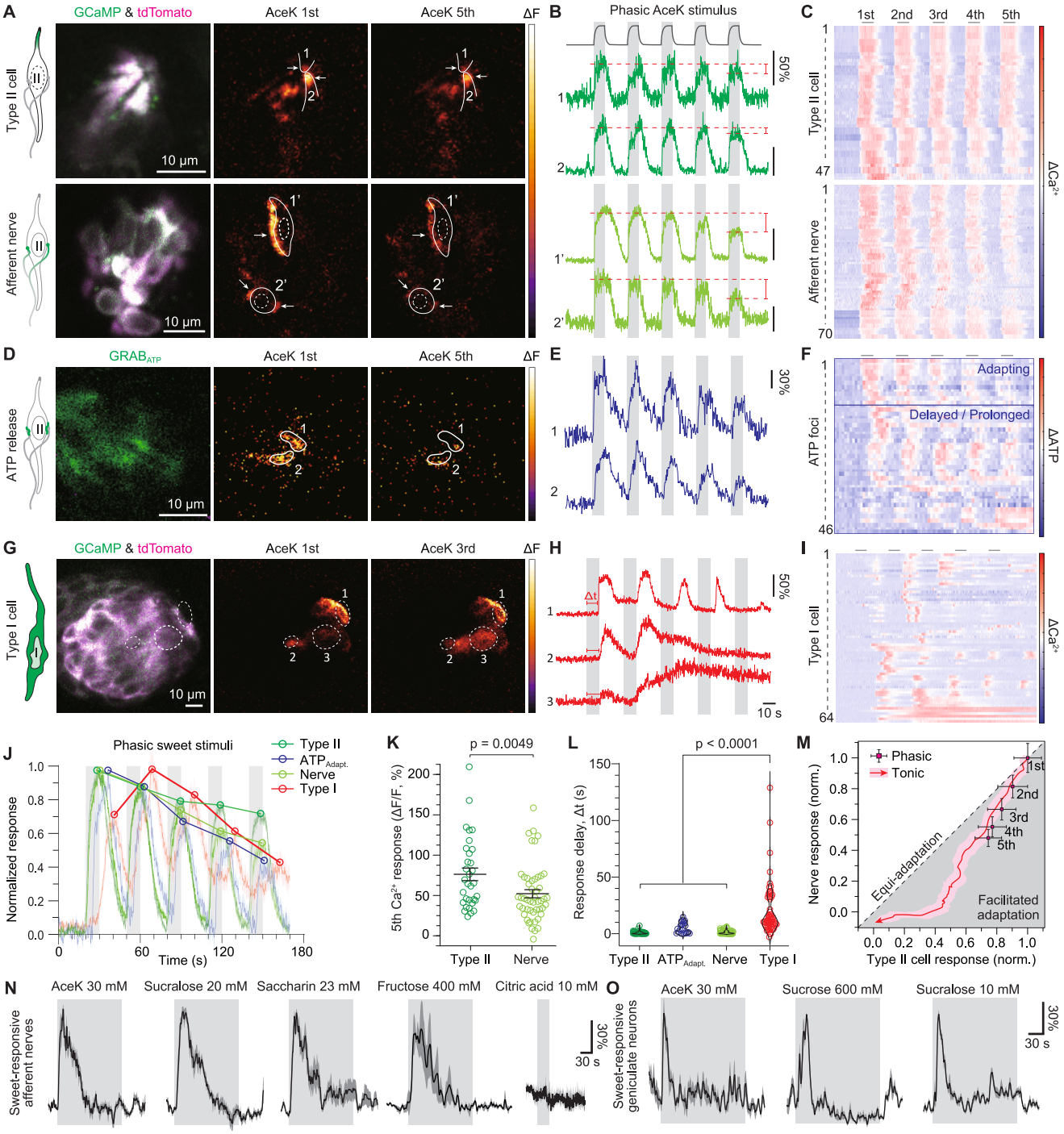

Figure S2. Cellular-subtype-specific functional dynamics in response to phasic sweet stimuli, related to Figure 1

(A) Representative calcium activity in type II cells (top) and afferent nerves (bottom) within a taste bud during a phasic sweet stimulus. The first column is the baseline fluorescence (F). The pseudocolored images represent the change in GCaMP fluorescence intensity (ΔF) in response to the repeated 30 mM AceK.

(B) Representative calcium activities of type II taste cells (dark green) and afferent nerves (light green) in (A). The shaded gray area represents the phasic AceK stimulus (10 s duration, 20 s interval, 5 repeats).

(C) Heatmap of functional calcium responses of type II cells (n = 47 cells) and afferent nerves (n = 70 nerves) during phasic sweet stimuli.

(D–F) Extracellular ATP release in response to phasic sweet stimuli measured in GAD2-GRAB$_{ATP}$ mice. n = 46 synaptic foci in (F). The data in (F) are sorted by the hierarchical clustering analysis. The three major clusters are indicated as adapting (n = 22 foci), non-adapting (n = 16 foci), and ramping (n = 8 foci).

(G–I) Type I cell activity in response to phasic sweet stimuli measured in GAD2-GCaMP6f-tdTomato mice (n = 64 cells in I).

(legend continued on next page)

(J) Summarized functional responses of type II cells (dark green), ATP release (purple), afferent nerves (light green), and type I taste cells (red) to phasic sweet stimuli, shaded in light gray.
(K) Comparison of the fifth responses in type II cells and afferent nerve, showing facilitated adaptation. $p = 0.0049$ by unpaired t test.
(L) Comparison of response delay (Δt) of type II cell, ATP release, afferent nerve, and type I cell. $p < 0.0001$ by one-way ANOVA test.
(M) Phase diagram illustrating the functional relationship between type II cell and afferent nerve responses during phasic and tonic sweet stimuli. The dotted line at "y = x" represents equi-adaptation, where the functional activity of a type II cell is equal to that of an afferent nerve. Both stimulus conditions consistently showed facilitated adaptation (shaded area; lower right side of the equi-adaptation line) with similar kinetics.
(N) Sweet adaptation to different sweet compounds. Afferent nerves in fungiform taste buds showed adapting kinetics to sucralose (20 mM), saccharine (23 mM), and fructose (400 mM), as well as AceK (30 mM). The sweet-responsive nerves did not respond to citric acid (10 mM). $n = 7$ cells from 2 mice.
(O) Sweet adaptation in the geniculate ganglion neurons to tonic stimulation of AceK (30 mM), sucrose (600 mM), and sucralose (10 mM).

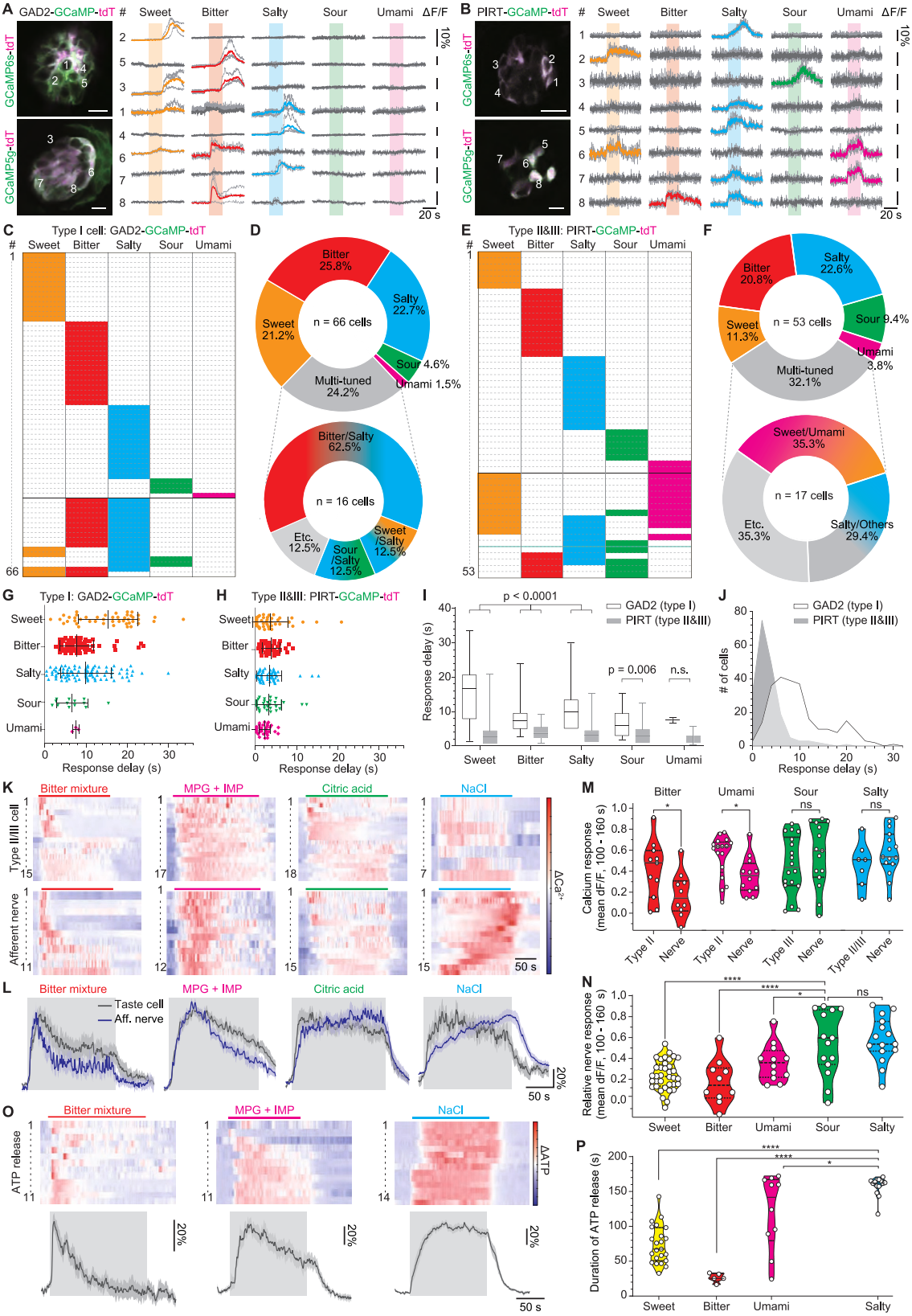

(legend on next page)

Figure S3. Comprehensive screening on other taste qualities, related to Figure 1

(A and B) Representative calcium responses of glia-like type I (GAD2-GCaMP-tdTomato mice) and chemosensory type II/III cells (PIRT-GCaMP-tdTomato mice). Sweet: 40 mM AceK. Bitter: 5 mM quinine, 5 mM denatonium, and 0.05 mM cycloheximide. Salty: 400 mM NaCl. Sour, 10 mM citric acid. Umami: 150 mM MPG and 1 mM IMP. Scale bar, 10 μm.

(C–F) Proportion of responses to single- and multi-tuned responses of taste bud cells. n = 66 type I cells for (C) and (D) and n = 53 type II/III cells for (E) and (F).

(G–J) Quantification of response delay in type I and type II/III cells. Note that the overall responses of type I cells are significantly delayed compared with those of type II/III cells. $p < 0.0001$ in sweet, bitter, salty; $p = 0.006$ in sour, n.s. in umami in (I) by unpaired t test.

(K) Heatmaps of taste cell and afferent nerve calcium responses to tonic stimuli (160 s) of tastant stimulation (bitter, umami, sour, and salty).

(L) Taste cell and afferent nerve activity (mean ± SEM) traces in response to tonic stimulation of other taste modalities.

(M) Quantitative analysis of mean dF/F values in normalized responses at time span of 100 to 160 s in taste cells and afferent nerves in other tastes (bitter, umami, sour, and salty).

(N) Quantitative analysis of mean dF/F values in normalized responses at time span of 100 to 160 s in afferent nerves for each taste (sweet, bitter, umami, sour, and salty).

(O) ATP release activity (mean ± SEM) in response to tonic stimulation of other taste modalities.

(P) Quantitative analysis of durations of prolonged responses in ATP release activity in tastes releasing ATP (sweet, bitter, umami, and salty).

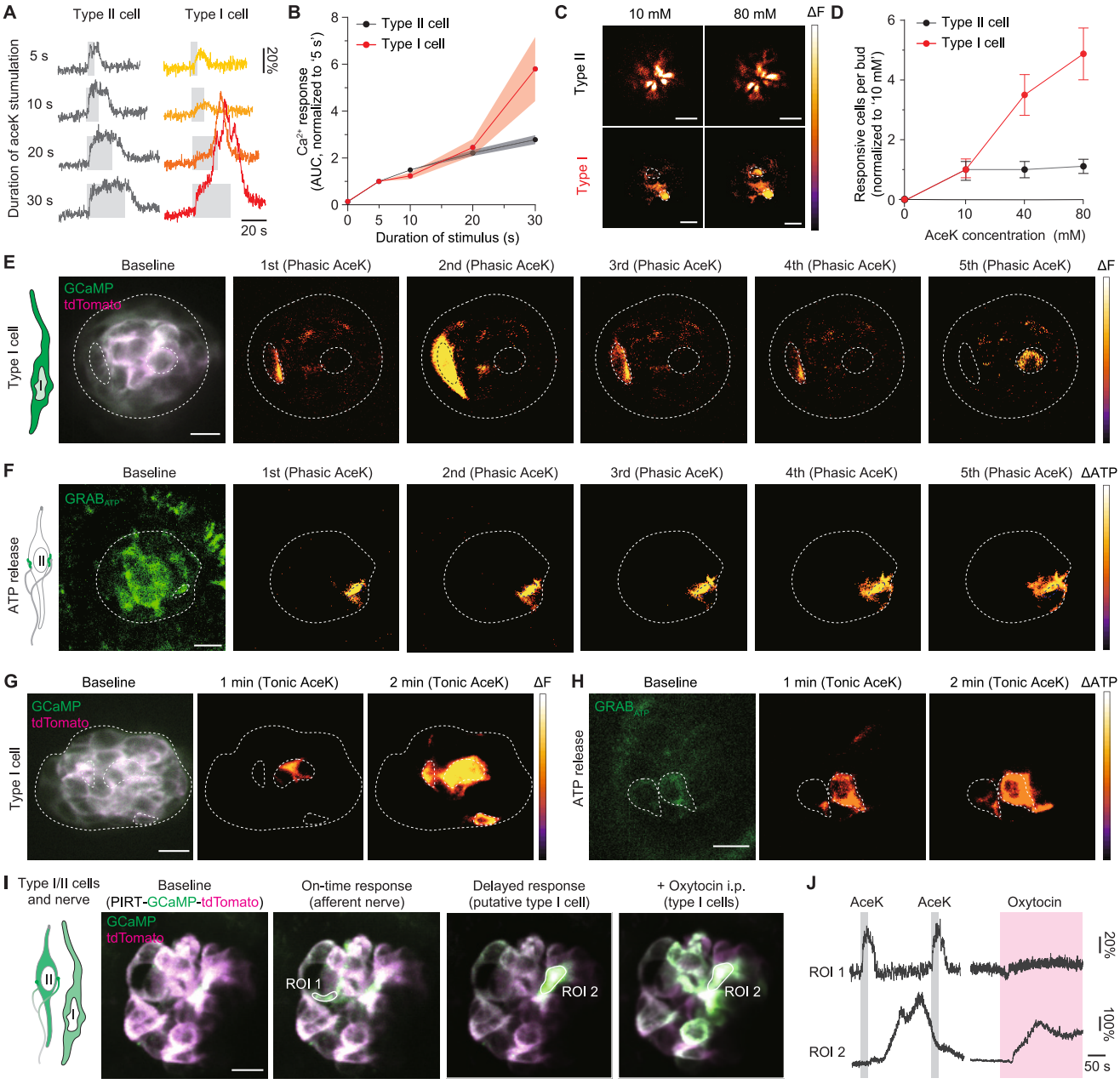

Figure S4. Type I cells show distinctive spatiotemporal dynamics deriving from extra-synaptic ATP input released by type II cells, related to Figure 1

(A and B) Sweet-evoked calcium responses of type II cells (left, $n = 11$ cells in 2 mice) and type I cells (right, $n = 6$ cells in 3 mice) in response to increasing duration of AceK stimulus (5, 10, 20, and 30 s). The area under curves in (B) are normalized to the Ca^{2+} response at 5 s. Type I cells show a distinctive progressive increase in the duration-response curve in (B).

(C and D) Number of responsive cells (type II: $n = 6$ buds, type I: $n = 33$ buds) with increasing AceK concentration.

(E) Spatial spread of type I cell calcium activity during phasic sweet stimulation at each stimulus. Dormant type I cell becomes active starting from the fifth stimulus.

(F) Spatial spread of ATP release at synaptic foci during phasic sweet stimulation at each stimulus, showing an expanding region of activity as stimuli accumulate.

(G) Spatial spread of type I cell calcium activity following 1 (middle) and 2 (right) min.

(H) Spatial spread of ATP release at synaptic foci following sweet stimulation of 1 (middle) and 2 (right) min of tonic sweet stimulation.

(I) Example case of leaky expression observed in PIRT-GCaMP6f-tdTomato mouse, demonstrating type I cell identification validation using intraperitoneal oxytocin (0.1 mg/kg) injection.

(J) Calcium response traces of individual cells in the PIRT-GCaMP6f-tdTomato taste bud. Region of interest (ROI) 1 shows robust responses to AceK with no response to oxytocin, while ROI 2 exhibits delayed and ramping response to AceK stimulation, also activated by oxytocin.

Scale bar, 10 μm in (C) and (E)–(I).

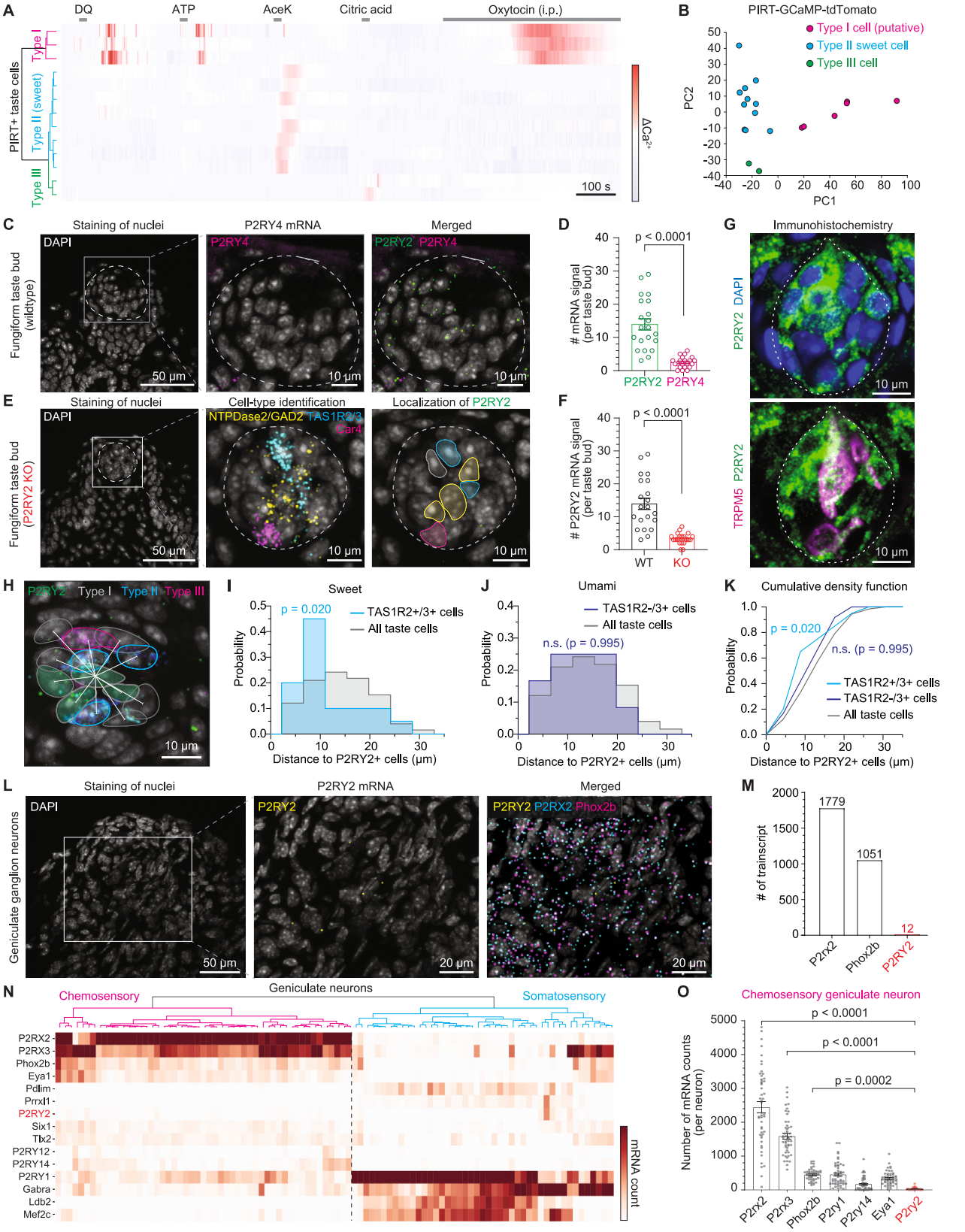

(legend on next page)

Figure S5. Specificity of P2RY2 in fungiform taste buds, related to Figure 3

(A) Calcium responses of taste cells observed in PIRT-GCaMP-tdTomato mice (n = 13 cells from 6 taste buds in 3 mice). Gray lines indicate the stimuli, including 5 mM diquafosol, 200 μM ATPγS, 30 mM AceK, 10 mM citric acid, and intraperitoneal oxytocin (0.1 mg/kg). Data are sorted by hierarchical clustering analysis.
(B) Principal-component analysis (PCA) using the area under curves of responses in (A).
(C) Representative images of a fungiform taste bud labeled with DAPI and mRNA FISH of P2RY2 and P2RY4.
(D) Quantification of mRNA puncta counts of P2RY2 and P2RY4 per taste bud slice (n = 2 mice).
(E) Representative image of a taste bud in P2RY2 knockout mouse, labeled with mRNA FISH of NTPDase2 and GAD2 (yellow), TAS1R2 (cyan), CAR4 (magenta), and P2RY2 (green).
(F) Quantification of mRNA signals of P2RY2 compared with wild-type (n = 2 mice) and P2RY2 knockout (n = 1 mouse) mouse models.
(G) Immunohistochemistry on DAPI (blue), P2RY2 (green), and TRPM5 (magenta) in a taste bud of a wild-type mouse.
(H) Image of taste bud labeled with DAPI and P2RY2 (green). Cell types were identified with NTPDase2+ as type I, TAS1R2+ and/or TAS1R3+ as type II, and CAR4+ as type III. Quantification of intercellular distances among taste bud cells. The intercellular distance was measured based on the center of mass of nuclei stained with DAPI.
(I and J) Probability density functions of intercellular distance between P2RY2+ type I cells and other cell types.
(K) Cumulative density function of distance to P2RY2+ type I cells. p = 0.020 for sweet cells, p = 0.995 for umami cells by Kolmogorov-Smirnov test.
(L) A representative mRNA FISH image of the geniculate ganglion with P2RY2 (yellow), P2RX2 (cyan), and Phox2b (magenta) probes.
(M) Quantification of detected mRNA spot counts in (L) by Airlocalize.
(N) Heatmap representation of raw reads from Dvoryanchikov et al.[65] scRNA-seq data. Single-cell RNAseq dataset available from GSE102443. Heatmap showing transcription level of cluster markers described in chemosensory and somatosensory neurons of the geniculate ganglion from Dvoryanchikov et al.[65]
(O) Quantification of the number of mRNA transcripts in chemosensory geniculate neurons in (N).

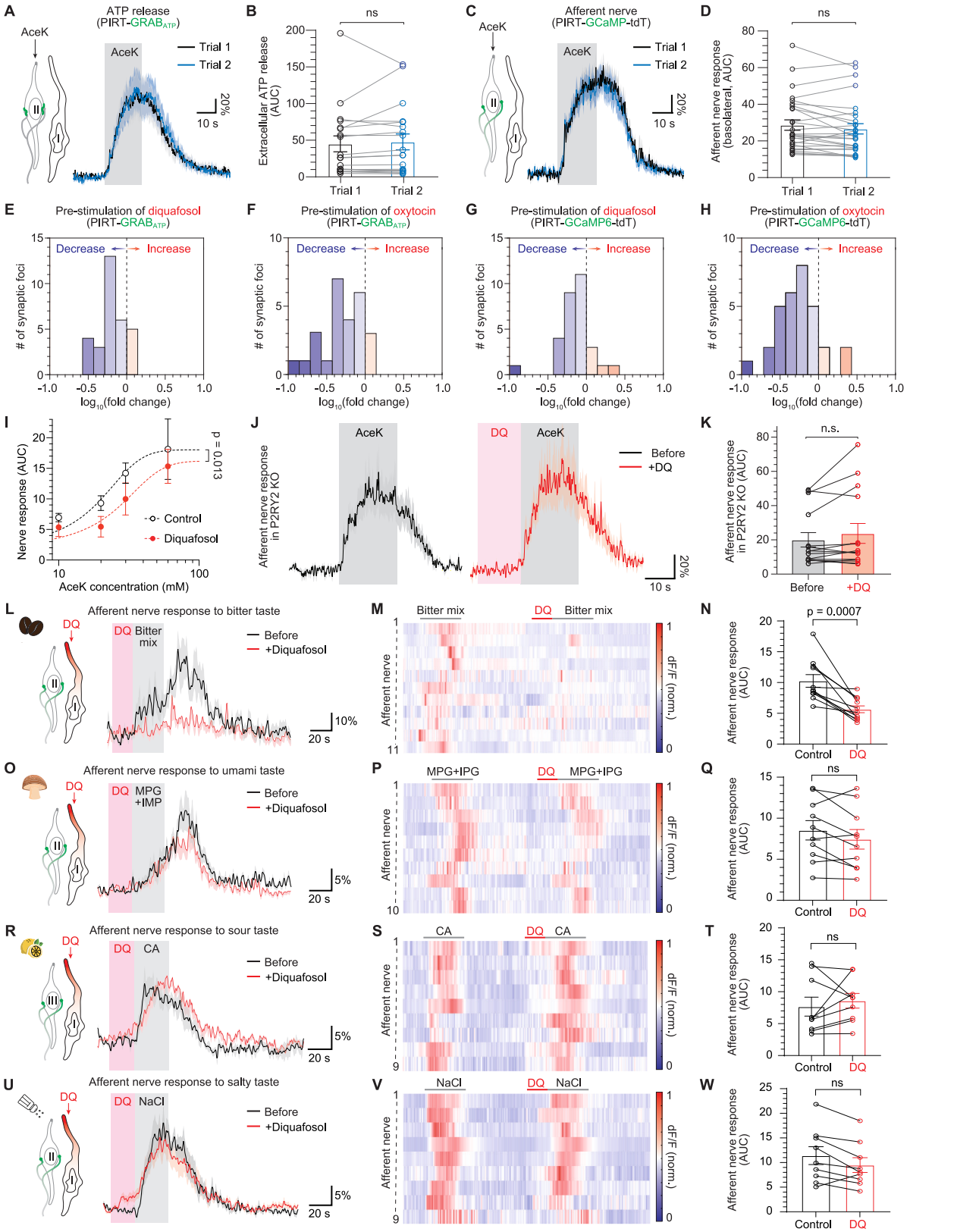

(legend on next page)

Figure S6. Purinergic activation of type I cells modulates taste information in a taste-modality-specific manner, related to Figure 4

(A and B) Robust ATP release (mean ± SEM) in response to the repeated 30 mM AceK trials (duration = 20 s, inter-trial interval = 10 min, gray bar). n.s. by paired t test in (B).

(C and D) Robust afferent nerve activity (mean ± SEM) in response to the repeated 30 mM AceK trials (duration = 20 s, inter-trial interval = 10 min, gray bar). n.s. by paired t test in (D).

(E–H) Histograms of fold change in ATP release (PIRT-GRAB$_{ATP}$) or nerve response (PIRT-GCaMP6-tdTomato) by diquafosol or oxytocin pre-treatments.

(I) Dose-response curve of afferent nerve calcium responses showing the control group and diquafosol group.

(J and K) The inhibitory effect of diquafosol was abolished in P2RY2 KO mice (n = 15 nerves in 5 mice). n.s. by Wilcoxon matched paired t test in (K).

(L–W) Inhibitory modulation of bitter-evoked nerve responses by diquafosol (5 mM). The influence of purinergic activation of type I cell on taste-evoked afferent nerve responses was measured in mice of which the gustatory afferents were labeled with AAV-PHP.S::CAG-GCaMP6. Note that only bitter taste showed significant inhibitory modulation by diquafosol (p = 0.0007 by paired t test); umami, sour, and salty tastes were not significantly affected (n.s. by paired t test).